THE JOURNAL OF PHYSICAL CHEMISTRY A

Article

Cite This: J. Phys. Chem. A 2019, 123, 631−649

pubs.acs.org/JPCA

Bath Gas Mixture Effects on Multichannel Reactions: Insights and Representations for Systems beyond Single-Channel Reactions

Lei Lei[†] and Michael P. Burke*[,‡]

[†]Department of Mechanical Engineering, Columbia University, New York, New York 10027, United States

[‡]Department of Mechanical Engineering, Department of Chemical Engineering, Data Science Institute, Columbia University, New York, New York 10027, United States

Supporting Information

ABSTRACT: Nearly all studies of and available data for pressure-dependent reactions focus on pure bath gases. Of the comparatively fewer studies on bath gas mixtures, important to combustion and planetary atmospheres, nearly all focus on single-channel reactions. The present study explores, and seeks reliable representations of, bath gas mixture effects on multichannel reactions. Analytical and numerical solutions of the master equation here reveal several unique manifestations of mixture effects for multichannel reactions, including behavior completely opposite to trends observed for single-channel reactions. The most common way of evaluating mixture rate constants from data for pure components, the classic linear mixture rule, is found to yield errors exceeding a factor of ∼10. A new linear mixture rule based on the reduced pressure, instead of the absolute pressure, is found to be accurate within ∼30% for rate constants (and ∼50% for the branching ratio). A new nonlinear mixture rule that additionally incorporates analytically derived activity coefficients is found to be accurate within ∼10% for rate constants and branching ratios. These new mixture rules are therefore recommended for use in fundamental and applied chemical kinetics investigations of reacting mixtures, including reacting flow codes and experimental interpretations of third-body efficiencies.

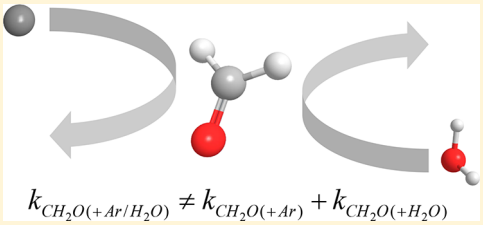

INTRODUCTION

A substantial fraction of the reactions that occur in combustion and planetary atmospheres proceed through rovibrationally excited intermediate complexes (i.e., "complex-forming" or "pressure-dependent" reactions). The fate of these complexes, and in turn the phenomelogical behavior that emerges from these reactions, is governed by the competition between reaction (unimolecular decomposition/isomerization[1−9] and even bimolecular reaction[10−16]) and energy transfer via collisions with the surrounding bath gas.

Most typical colliders in practice are generally "weak", in the sense that they transfer only a limited amount of energy per collision.[4,17,18] Consequently, except in the high-pressure limit, rate constants for complex-forming reactions are often different for different bath gases, which may transfer different amounts of energy on average in collisions. In many practical mixtures, there are multiple components with varied energy transfer characteristics present in sizable fractions, especially in combustion where many fuels (e.g., CH_4) and products (e.g., H_2O and CO_2), known to be much stronger colliders than O_2 and N_2 in air, are present in sufficient amounts to contribute significantly to collisional energy transfer.

The vast majority of experimental and theoretical studies of and available data for rate constants of complex-forming reactions, however, mainly focus on reactions in pure bath gases. Thereafter, rate constants in mixtures are almost always evaluated via a "mixture rule", which estimates the rate constant in the mixture from available data for rate constants in pure bath gases. Such mixture rules both comprise important elements of reacting flow codes[19−24] and play a role in experimental determinations of third-body efficencies.[25,25−28] Therefore, quantifying, and improving, the accuracy and generality of mixture rules in representing multicomponent pressure dependence is of great significance to fundamental and applied chemical kinetics investigations.

Understanding mixture effects has historically been a subject of considerable attention for single-channel, single-well unimolecular reactions.[29−41] These studies identified a number of key trends regarding mixture effects for single-channel reactions that provide useful insights when rate constants are predicted and experimental data are interpreted in mixtures. First of all, the rate constant in a mixture is, in general, not a simple linear sum of the contributions of individual components, thus implying a nonlinear mixture rule.[29,30] Second, the classic linear mixture rule (cf. LMR,P in Table 2) always underestimates the rate constant in the mixture,[30] i.e., any nonzero deviations from the classic linear mixture rule are always positive. Third, deviations from the classic linear mixture rule are generally larger when mixture components have greater differences in their energy transfer characteristics. Fourth, deviations of the classic linear mixture rule (LMR,P) peak in the intermediate falloff regime, reaching errors of

Received: October 30, 2018
Revised: December 21, 2018
Published: December 26, 2018

DOI: 10.1021/acs.jpca.8b10581
J. Phys. Chem. A 2019, 123, 631−649

~60% compared to master equation calculations for H + O_2 (+M) = HO_2 (+M).[41] By contrast, two newly proposed reduced-pressure-based mixture rules (cf. LMR,R and NMR,R in Table 2) reduce the maximum deviations to within ~10% (LMR,R) and ~3% (NMR,R).[41]

Even though nearly all previous studies on mixture effects have focused on single-channel, single-well reactions, many, if not most, important complex-forming reactions proceed through multiple wells and/or multiple channels. In our previous work,[42] we assessed the performance of various mixture rules for the multichannel allyl + HO_2 reaction and explored the implications of mixture effects for this reaction for combustion modeling. We found that, for this reaction, generalized versions of the reduced-pressure mixture rules developed for single-channel reactions[41] better reproduced master equation calculations than the classic linear mixture rule. In general, however, compared to single-channel reactions, considerably less is known about both mixture effects and general applicability of mixture rules for multichannel reactions.

As will be demonstrated below, certain trends and conclusions regarding mixture effects drawn from single-channel, single-well reactions are not directly transferable to their multichannel counterparts. In fact, naive application of these conclusions to multichannel reactions, in many cases, can lead to entirely opposite behavior than observed. For example, in contrast to the conclusions for single-channel systems, we find that the classic linear mixture rule overestimates, rather than underestimates, rate constants for some channels; additionally, deviations from the linear mixture rule in the low-pressure limit for some channels show a nonmonotonic, rather than monotonic, dependence on the average energy transferred per collision. Furthermore, the maximum deviations from mixture rules can be considerably more pronounced, reaching a factor of ~10. In general, understanding the key trends, and origins, of mixture effects for multichannel reactions requires further attention, especially given the importance of reliable mixture rules for accurate kinetic modeling and experimental interpretations in mixtures.

Here, we present analytical solutions to the master equation in the low-pressure limit for a multichannel reaction in a multicomponent bath gas in order to derive activity coefficients, f_i, that can be used in the most accurate nonlinear mixture rules (Table 2). This analysis extends previous derivations of activity coefficients by Troe[29] for a single-channel reaction in a two-component bath gas to an arbitrary N-channel reaction in an M-component bath gas. We then compare the performance of the classic linear mixture rule and two newly proposed, reduced-pressure-based mixture rules against numerical solutions of master equation for formaldehyde (CH_2O) decomposition, a prototypical multichannel reaction. In the accompanying discussion, we use the analytical and numerical solutions to explain the observed trends and understand the observed differences from those of single-channel reactions.

■ ANALYTICAL AND COMPUTATIONAL METHODS

Analytical Solutions of the Master Equation in the Low-Pressure Limit. The section below presents analytical solutions to the master equation in the low-pressure limit for a single-well multichannel unimolecular reaction taking place in a multicomponent mixture. The analysis builds on previous analytical solutions to the master equation in the low-pressure limit for single-channel reactions in a two-component collider by Troe[29] and for two-channel reactions in a single-component collider by Just and Troe.[43] The first section below presents analysis for a multichannel reaction with an arbitrary number of channels in a single-component bath gas, in order to obtain expressions for channel-specific rate constants for a given single-component bath gas. The second section then presents analysis for a multichannel reaction with an arbitrary number of channels in a bath gas consisting of an arbitrary number of components, in order to determine how the channel-specific rate constants in the bath gas mixture are related to channel-specific rate constants of each bath gas component in isolation. The analysis below, similar to previous analyses,[29,43,44] considers an energy-resolved master equation for a reactant highly diluted in an inert bath gas.

Multichannel Reactions in a Single-Component Bath Gas. The time evolution of the concentration of reactants with vibrational energy E, denoted by $n(E,t)$, in a pure inert bath gas, M_i, under conditions where reverse reactions from bimolecular products to reactant can be ignored (which is actually not so restrictive, as discussed below), can be described by the master equation

$$\frac{dn(E,t)}{dt} = Z_i\cdot[M_i]\int_0^{+\infty} P_i(E,E')\cdot n(E',t)\,dE' - Z_i\cdot[M_i]\cdot n(E,t) - k_p(E)\cdot n(E,t) \quad (1)$$

where Z_i is the collision frequency between the reactant and M_i (taken to be energy-independent as is common), $[M_i]$ is the concentration of pure inert bath gas consisting of only species i, $P_i(E,E')$ is the probability that a given collision between the reactant and M_i induces a transition from the reactant with energy E' to that with energy E such that $Z_i\cdot P_i(E,E')$ gives the second-order collisional energy transfer rate constants $k_i(E,E')$, and $k_p(E)$ is the total microcanonical decomposition rate constant of the reactant with energy E, is the sum of the N channel-specific rate constants, $k_{p,j}(E)$, i.e., $k_p(E) = \sum_j k_{p,j}(E)$. Detailed balance for $k_i(E,E')$ then requires that

$$Z_i\cdot P_i(E,E')\cdot f(E') = Z_i\cdot P_i(E',E)\cdot f(E) \quad (2)$$

where $f(E)$ denotes the Boltzmann (thermal equilibrium) distribution

$$f(E) = \frac{\rho(E)\exp(-E/k_BT)}{\int_0^{+\infty}\rho(E')\exp(-E'/k_BT)\,dE'} \quad (3)$$

with the density of states of the reactant, $\rho(E)$, the Boltzmann constant, k_B, and the temperature, T.

Upon introducing a nonequilibrium population factor, $h_i(E,t)$, which measures the deviation of the normalized population of the reactant at a given time from the thermal equilibrium distribution, $f(E)$,[44]

$$h_i(E,t) = \frac{n(E,t)}{\int_0^{+\infty} n(E',t)\,dE'\cdot f(E)} \quad (4)$$

the master equation (1) can be recast using eqs 2 and 4 as

$$\frac{dh_i(E,t)}{dt} = Z_i\cdot[M_i]\int_0^{+\infty} P_i(E',E)\cdot h_i(E',t)\,dE' - (Z_i\cdot[M_i] + k_p(E) - k)\cdot h_i(E,t) \quad (5)$$

where the pseudo-first-order rate constant for total decomposition k is defined as

DOI: 10.1021/acs.jpca.8b10581
J. Phys. Chem. A 2019, 123, 631−649

$$k = -\frac{1}{\int_0^{+\infty} n(E',t)\,\mathrm{d}E'}\frac{\mathrm{d}\left(\int_0^{+\infty} n(E',t)\,\mathrm{d}E'\right)}{\mathrm{d}t} \tag{6}$$

Under conditions where a phenomenological description applies, the time scale for reaction, $1/k$, is sufficiently long relative to time scales for internal energy relaxation that there is a period over which the reaction proceeds with a time-independent rate constant suitable for use in phenomenological kinetic models. During this period for single-well decomposition reactions, the nonequilibrium population factor has reached a quasi-steady-state distribution, i.e., $dh_i(E,t)/dt \approx 0$. Under such conditions, the decomposition rate, k, is usually much less than the collision rate, $Z_i\cdot[M_i]$, such that $(Z_i\cdot[M_i]-k) \approx Z_i\cdot[M_i]$. (Similarly, under such conditions, decomposition rate constants calculated neglecting reverse reactions are also applicable to situations where reverse reactions are non-negligible, as discussed elsewhere.[45−47])

For reactants with energies below the lowest decomposition threshold $E_{01}^{\dagger}$, $E < E_{01}^{\dagger}$ (i.e., stable states), the microcanonical rate is identically zero, $k_p(E) = 0$. Likewise, for reactants with energies above the lowest decomposition threshold, $E > E_{01}^{\dagger}$ (i.e., unstable stables), the microcanonical rate is nonzero and in the low-pressure limit, where the collision rate approaches zero, the microcanonical rate greatly exceeds the collision rate and $(Z_i\cdot[M_i] + k_p(E)) \approx k_p(E)$. Consequently, in the low-pressure limit, the quasi-steady-state distribution for the nonequilibrium population factor becomes

$$h_i(E) = \begin{cases} \displaystyle\int_0^{\infty} P_i(E',E)\,h_i(E')\,\mathrm{d}E' & E < E_{01}^{\dagger} \\ \displaystyle\frac{Z_i\cdot[M_i]}{k_p(E)}\int_0^{\infty} P_i(E',E)\,h_i(E')\,\mathrm{d}E' & E > E_{01}^{\dagger} \end{cases} \tag{7}$$

Equation 7 can be further simplified by recognizing that in the low-pressure limit, as per eq 7, $h_i(E>E_{01}^{\dagger}) \ll h_i(E<E_{01}^{\dagger})$ and the upper limits of integration are effectively truncated from $+\infty$ to $E_{01}^{\dagger}$ yielding[44]

$$h_i(E) = \begin{cases} \displaystyle\int_0^{E_{01}^{\dagger}} P_i(E',E)\,h_i(E')\,\mathrm{d}E' & E < E_{01}^{\dagger} \\ \displaystyle\frac{Z_i\cdot[M_i]}{k_p(E)}\int_0^{E_{01}^{\dagger}} P_i(E',E)\,h_i(E')\,\mathrm{d}E' & E > E_{01}^{\dagger} \end{cases} \tag{8}$$

Once a collisional energy transfer probability function, $P_i(E',E)$, is specified, eq 8 can be used to calculate the quasi-steady-state nonequilibrium population factor, $h_i(E)$, in the low-pressure limit and the channel-specific rate constants for each of the N channels can be calculated via[43]

$$k_{j,i} = \int_{E_{01}^{\dagger}}^{+\infty} k_{p,j}(E)\,h_i(E)\,f(E)\,\mathrm{d}E \tag{9}$$

The commonly employed exponential-down model is used here to describe the collisional energy transfer function to facilitate analytical solutions that permit straightforward interpretations and to allow compatibility of the activity coefficients so-obtained with the vast majority of calculated rate constants (which use the same model). (In reality, collisional energy transfer functions with more complex E dependence as well as J, angular momentum, dependence have been shown to better represent results from experimental measurements and trajectory calculations.[4,8,17,48−53] Improved quantification of mixture effects in the future would be achieved using more representative collisional energy transfer functions, particularly as more becomes known about their associated parameters for different bath gases.)

In the exponential-down model, the collisional energy transfer probability function, $P_i(E',E)$, describing down collisions for the ith collider is given by

$$P_i(E',E) = \frac{1}{\eta}\exp\left(-\frac{E-E'}{\alpha_i}\right) \qquad E > E' \tag{10}$$

where η is a normalization constant such that the integral of $P_i(E',E)$ over all E is unity and α_i is the average energy transferred per down collision ($E > E'$). The collisional energy transfer probability function, $P_i(E,E')$, for up collisions ($E < E'$) is then prescribed by detailed balance eq 2. Assuming that α_i is sufficiently small relative to energies of interest to kinetics (e.g., those near $E_{01}^{\dagger}$), as is often the case, then integrals with lower integration limits of 0 can be well approximated by integrals with lower integration limits of $-\infty$.[44] Furthermore, assuming that the energy dependence of the density of states, $\rho(E)$, near the lowest decomposition threshold can be reasonably approximated locally as an exponential function of E characterized by a factor F_E describing the energy dependence of the density of states

$$F_E = \frac{\int_{E_{01}^{\dagger}}^{+\infty}\rho(E)\exp(-E/k_BT)\,\mathrm{d}E}{\rho(E_{01}^{\dagger})\exp(-E_{01}^{\dagger}/k_BT)k_BT} \tag{11}$$

such that

$$\rho(E) = \rho(E_{01}^{\dagger})\exp\left(\frac{(F_E-1)(E-E_{01}^{\dagger})}{F_Ek_BT}\right) \tag{12}$$

then the collisional energy transfer probability function, $P_i(E',E)$, can be expressed as[44]

$$P_i(E',E) = \begin{cases} \displaystyle\frac{1}{\alpha_i+\gamma_i}\exp\left(-\frac{E-E'}{\alpha_i}\right) & E > E' \\ \displaystyle\frac{1}{\alpha_i+\gamma_i}\exp\left(-\frac{E'-E}{\gamma_i}\right) & E < E' \end{cases} \tag{13}$$

where γ_i is the average energy transferred per up collision and detailed balance eq 2 dictates that α_i and γ_i are related through a weighted Boltzmann factor,[44] F_Ek_BT:

$$\gamma_i = \alpha_iF_Ek_BT/(\alpha_i + F_Ek_BT) \tag{14}$$

Equations 8 and 13 suggest a solution for $h_i(E)$ for $E < E_{01}^{\dagger}$ of the form[44]

$$h_i(E) = 1 - C\cdot\exp\left(-\frac{E_{01}^{\dagger}-E}{D}\right) \qquad E \le E_{01}^{\dagger} \tag{15}$$

where substitution of eq 15 into eq 8 for $E < E_{01}^{\dagger}$ yields values for the coefficients of $C = \alpha_i/(\alpha_i + F_Ek_BT)$ and $D = F_Ek_BT$. Further substitution of eq 15 with these coefficients into eq 8 for $E > E_{01}^{\dagger}$ yields the nonequilibrium population factor above the decomposition threshold, altogether resulting in

DOI: 10.1021/acs.jpca.8b10581
J. Phys. Chem. A 2019, 123, 631−649

$$h_i(E) = \begin{cases} 1 - \dfrac{F_E k_B T}{\alpha_i + F_E k_B T} \exp\left(-\dfrac{E_{01}^{\dagger}}{F_E k_B T}\right) & E \le E_{01}^{\dagger} \\ \left(\dfrac{Z_i[M_i]}{k_p(E)}\right)\left(\dfrac{\alpha_i}{\alpha_i + F_E k_B T}\right) & E > E_{01}^{\dagger} \\ \quad \exp\left(-\dfrac{E - E_{01}^{\dagger}}{\alpha_i}\right) \end{cases} \tag{16}$$

Finally, by substituting eq 16 into eq 9, the channel-specific rate constant for the jth decomposition channel in a single component collider i can be expressed as

$$k_{j,i} = Z_i[M_i]\frac{\alpha_i}{\alpha_i + F_E k_B T}\int_{E_{0j}^{\dagger}}^{\infty} \frac{k_{p,j}(E)}{\sum_n k_{p,n}(E)} \exp\left(-\frac{E - E_{01}^{\dagger}}{\alpha_i}\right) f(E)\, dE \tag{17}$$

Multichannel Reactions in Multicomponent Bath Gases. The master equation can be expressed for the same single-well multichannel reaction taking place instead in a bath gas consisting of M different components given by

$$\frac{dn(E,t)}{dt} = \sum_{i=1}^{M} Z_i \cdot [M_i] \int_0^{+\infty} P_i(E,E') \cdot n(E',t)\, dE' - \left(\sum_{i=1}^{M} Z_i \cdot [M_i] + k_p(E)\right) \cdot n(E,t) \tag{18}$$

where the subscript i refers to the ith component of the bath gas. Following a similar analysis to that above, eq 18 can be recast in terms of the nonequilibrium population factor, $h(E,t)$, defined in eq 4, viz.

$$\frac{dh(E,t)}{dt} = \sum_{i=1}^{M} Z_i \cdot [M_i] \int_0^{+\infty} P_i(E',E)\, h(E',t)\, dE' - \left(\sum_{i=1}^{M} Z_i \cdot [M_i] + k_p(E) - k\right) h(E,t) \tag{19}$$

and, in the low-pressure limit, the quasi-steady-state non-equilibrium population factor, $h(E)$, becomes

$$h(E) = \begin{cases} \displaystyle\sum_{i=1}^{M} \hat{X}_i \int_0^{E_{01}^{\dagger}} P_i(E',E)\, h(E')\, dE' & E < E_{01}^{\dagger} \\ \displaystyle\sum_{i=1}^{M} \frac{Z_i[M_i]}{k_p(E)} \int_0^{E_{01}^{\dagger}} P_i(E',E)\, h(E')\, dE' & E > E_{01}^{\dagger} \end{cases} \tag{20}$$

where $\hat{X}_i = Z_i[M_i]/\sum_n Z_n[M_n]$ is the collision-frequency-weighted mole fraction for the ith collider. Again, eqs 13 and 20, suggest a solution for $E < E_{01}^{\dagger}$ of the form

$$h(E) = 1 - \sum_{i=1}^{M} C_i \cdot \exp\left(-\frac{E_{01}^{\dagger} - E}{D_i}\right) \qquad E < E_{01}^{\dagger} \tag{21}$$

and substitution of eq 21 into eq 20 suggests that the coefficients C_i and D_i must satisfy

$$\begin{cases} \displaystyle\sum_{m=1}^{M} \frac{\hat{X}_m D_i}{\alpha_m + \gamma_m}\left(\frac{\alpha_m}{\alpha_m + D_i} - \frac{\gamma_m}{\gamma_m - D_i}\right) - 1 = 0 \\ \displaystyle\sum_{n=1}^{M} \frac{C_n D_n}{\gamma_i - D_n} + 1 = 0 \end{cases} \tag{22}$$

The coefficients can be found by first solving for M roots of the first equation for which $D_i > 0$ and then substituting these values for each D_i into the second equation to yield a linear system with respect to the pre-exponential coefficients C_i whereby each C_i can be found. (Note that the number of each possible C_i and D_i equals the total number of mixture components, but each does not necessarily, and often does not, correspond to any individual component.) Further substitution of eq 21 and these coefficients into eq 20 for $E > E_{01}^{\dagger}$ yields the nonequilibrium population factor above the decomposition threshold, altogether giving

$$h(E) = \begin{cases} 1 - \displaystyle\sum_{i=1}^{M} C_i \cdot \exp\left(-\frac{E_{01}^{\dagger} - E}{D_i}\right) & E < E_{01}^{\dagger} \\ \displaystyle\sum_{i=1}^{M} \frac{Z_i[M_i]}{k_p(E)} \frac{\alpha_i}{\alpha_i + \gamma_i}\left(1 - \sum_{m=1}^{M} \frac{C_m D_m}{\alpha_i + D_m}\right) \cdot & E > E_{01}^{\dagger} \\ \quad \exp\left(-\dfrac{E - E_{01}^{\dagger}}{\alpha_i}\right) \end{cases} \tag{23}$$

By substitution of eq 23 into eq 9, the channel-specific rate constant for the jth decomposition channel in the bath gas mixture, $k_{j,\mathrm{mix}}$, can be expressed as

$$k_{j,\mathrm{mix}} = \sum_{i=1}^{M}\left[\frac{\alpha_i + F_E k_B T}{\alpha_i + \gamma_i}\left(1 - \sum_{m=1}^{M} \frac{C_m D_m}{\alpha_i + D_m}\right)\right] \cdot \left[Z_i[M_i]\frac{\alpha_i}{\alpha_i + F_E k_B T} \times \int_{E_{0j}^{\dagger}}^{+\infty} \frac{k_{p,j}(E)}{\sum_m k_{p,m}(E)} \exp\left(-\frac{E - E_{01}^{\dagger}}{\alpha_i}\right) f(E)\, dE\right] \tag{24}$$

Recognizing the second term in large brackets as the corresponding channel-specific rate constant in a bath gas consisting of the ith component in isolation, $k_{j,i}$ (cf. eq 17), the rate constant in the mixture can be related to rate constants in the constituent components in isolation through

$$k_{j,\mathrm{mix}} = \sum_{i=1}^{M} k_{j,i} f_i \tag{25}$$

where each activity coefficient,[29] f_i, is given by

$$f_i = \frac{\alpha_i + F_E k_B T}{\alpha_i + \gamma_i}\left(1 - \sum_{m=1}^{M} \frac{C_m D_m}{\alpha_i + D_m}\right) \tag{26}$$

Interestingly, as shown by eq 26, the activity coefficient for the ith collider, f_i, only depends on the properties of colliders and mixture composition and is the same for each channel. (In fact, for a two-component mixture ($M = 2$), eqs 22 and 26 yield the same activity coefficients as previously derived by Troe[29] for a single-channel reaction in a two-component mixture, shown in the Supporting Information). However, eqs 25 and 26 do not imply that the deviations from the linear mixture rule will be the same magnitude, or even the same sign, for each channel because each collider may have a different

DOI: 10.1021/acs.jpca.8b10581
J. Phys. Chem. A 2019, 123, 631−649

fractional contribution to each channel. In fact, the results below indicate that the linear mixture rule underestimates the rate constant for the lower energy channel whereas it overestimates the rate constant for the higher energy channel in the low-pressure limit. In general, the activity coefficients, f_i, are nonunity quantities as long as $M > 1$, such that, except in special cases, eqs 25 and 26 imply a nonlinear, rather than linear, mixture rule (consistent with previous studies on single-channel systems[29,30,41]).

Before investigating these limiting cases, it is helpful to transform eq 22 into

$$\sum_{m=1}^{M}\left[\frac{1}{1+\frac{{\alpha_m}^2}{(\alpha_m+F_E k_B T)D_i}-\frac{{\alpha_m}^2 F_E k_B T}{(\alpha_m+F_E k_B T){D_i}^2}}\right]\hat{X}_m = 1 \tag{27}$$

which indicates that $D_i = F_E k_B T$ is always a root to this equation. It can also be further shown that all positive roots of D_i must not greater than $F_E k_B T$ (otherwise the summation would be smaller than unity). Similarly, on this basis, at least one term in the bracket in front of $\hat{X}_m$ in eq 27 must be negative (otherwise the summation would be greater than unity). That is, $\forall\ D_i \neq F_E k_B T$ (as the term in the bracket in eq 27 for $D_i = F_E k_B T$ is always unity), where $\forall\ D_i \neq F_E k_B T$ denotes "for all D_i not equal to $F_E k_B T$", there must exist some $q \in \{1, 2, ..., M\}$ such that

$$\frac{1}{1+\frac{{\alpha_q}^2}{(\alpha_q+F_E k_B T)D_i}-\frac{{\alpha_q}^2 F_E k_B T}{(\alpha_q+F_E k_B T){D_i}^2}} < 0 \tag{28}$$

Solving the quadratic inequality eq 28 yields an upper bound for each $D_i \neq F_E k_B T$ of γ_q for some q. Given that $\gamma_i < F_E k_B T\ \forall\ i$ (cf. eq 14), γ_{max} (where $\gamma_{max} = \max\{\gamma_i|i=1,2,...,M\}$) is an upper bound for all $D_i \neq F_E k_B T$. Similarly, there must exist some other $q \in \{1, 2, ..., M\}$ such that the term in the bracket in eq 27 in front of $\hat{X}_q$ is positive. Repeating the same procedure for the corresponding inequality gives a lower bound for D_i of $\gamma_{min}\ \forall\ D_i \neq F_E k_B T$ (where $\gamma_{min} = \min\{\gamma_i|i=1,2,...,M\}$). Taking the intersection of two domains implies that all D_i's other than $F_E k_B T$ are bounded in the range

$$D_i \in [\gamma_{min}, \gamma_{max}] \tag{29}$$

The following limiting cases are interesting to explore:

(1) If all the colliders have identical exponential-down factors but different collision frequencies, i.e., $\alpha_1 = \alpha_2 = \cdots = \alpha_M = \alpha$ but $Z_i \neq Z_j$ for $i \neq j$, eq 27 becomes

$$-\frac{{D_i}^2(\alpha+F_E k_B T)}{(\alpha+D_i)[\alpha F_E k_B T-(\alpha+F_E k_B T)D_i]}\sum_{m=1}^{M}\hat{X}_m = 1 \tag{30}$$

Given that $\sum_{m=1}^{M}\hat{X}_m = 1$, the preceding term in eq 30 must also equal 1. In this case, one can solve for D_i explicity, which yields only one existing root equal to $D_i = F_E k_B T$. From the expression for C_i in eq 22, the corresponding C_i can be shown to be $C_i = (F_E k_B T)/(\alpha + F_E k_B T)$. Therefore, $h(E)$ in eq 23 below $E_{01}^{\dagger}$ equivalently reduces to its single-component counterpart $h_i(E)$ of eq 16. (After all, in the low-pressure limit, the subthreshold energy distribution is independent of the collision rate, which is the only difference among colliders with the same α.) Likewise, the activity coefficients of eq 26 reduce to unity, such that the linear mixture rule is exact.

(2) If the strong-collision limit holds for all colliders in the mixture such that $\alpha_i \gg F_E k_B T$ for $i = 1, 2, ..., M$, we have $\gamma_i = (\alpha_i F_E k_B T)/(\alpha_i + F_E k_B T) \to F_E k_B T\ \forall\ i$ and from eq 29 it follows that $D_i \to F_E k_B T\ \forall\ i$. Similarly, given that $D_i/(\gamma_m - D_i) \to \pm\infty$, eq 22 implies that $C_i \to 0\ \forall\ i$ (otherwise the summation would approach $\pm\infty$ rather than -1). As a result, $h(E) = 1$ below $E_{01}^{\dagger}$, which is simply the thermally equilibrated Boltzmann distribution $f(E)$ (equivalent to the single-component strong collision limit), such that differences in α_i among mixture components have no significant impact on the energy distribution. Therefore, according to eq 26, all f_i approach unity to yield a linear mixture rule $k_{j,mix} \approx \sum_i k_{j,i}$.

(3) If the weak-collision limit is instead achieved for all colliders, i.e., $\alpha_i \ll F_E k_B T\ \forall\ i$, then $\gamma_i = \frac{\alpha_i F_E k_B T}{\alpha_i + F_E k_B T} \to \alpha_i \ll F_E k_B T\ \forall\ i$. Given the bounds for D_i's other than $F_E k_B T$ in eq 29, all $D_i \neq F_E k_B T$ in eq 21 would approach zero. Furthermore, if one takes $D_1 = F_E k_B T$, then the constraint on C_i from eq 22 can be rewritten as

$$\sum_{n=2}^{M}\frac{C_n D_n}{\gamma_i - D_n} = -1 + \frac{C_1}{1-\gamma_i/F_E k_B T}\ \forall\ i \tag{31}$$

Subtracting eq 31 for i where $\gamma_i = \gamma_{max}$ from eq 31 for i where $\gamma_i = \gamma_{min}$ then yields

$$\sum_{n=2}^{M}\frac{C_n D_n}{\gamma_{max} - D_n} - \sum_{n=2}^{M}\frac{C_n D_n}{\gamma_{min} - D_n} = \frac{C_1}{1-\gamma_{max}/F_E k_B T} - \frac{C_1}{1-\gamma_{min}/F_E k_B T} \tag{32}$$

where given that $\gamma_i/F_E k_B T \to 0\ \forall\ i$ in the weak collision limit, the denominators in both terms on the right-hand side approach unity and therefore the entire right-hand side approaches zero in the weak collision limit. From eq 29, since $C_i \geq 0\ \forall\ i$, it follows that all the terms in the first summation are positive and all the terms in the second summation are negative, such that all terms on the left-hand side are positive. Therefore, eq 32 requires that $C_i \to 0\ \forall\ i \neq 1$, which together with eq 31 requires that $C_1 \to 1$ in the weak collision limit. As a result, $h(E) \to 1 - \exp(-(E_{01}^{\dagger} - E)/F_E k_B T)$ below $E_{01}^{\dagger}$, which collapses onto its single-component counterpart $h_i(E)$ in the weak collision limit. Interestingly, from numerical solutions with decreasing ratios of $\alpha_i/F_E k_B T$, it appears that activity coefficients do not approach unity but deviations of the linear mixture rule still approach zero for all channels in the weak collision limit (cf. Figure 3c below).

Numerical Solutions of the Master Equation. To demonstrate the key features of mixture effects and assess mixture rules for multichannel reactions, the CH_2O system (Figure 1), a single-well two-channel system often used as a

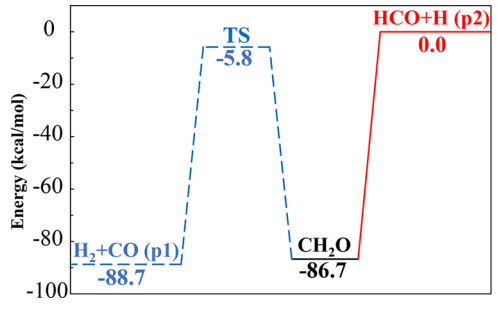

Figure 1. Potential energy surface of the CH_2O system.[54]

DOI: 10.1021/acs.jpca.8b10581
J. Phys. Chem. A 2019, 123, 631−649

prototypical multichannel reaction, is selected as a case study. Master equation calculations are performed using the PAPR-MESS code[9] using the potential energy surface from Klippenstein.[54] Similar to many other decomposition systems, CH_2O decomposition can occur through a lower energy tight transition state to produce two stable products (H_2 + CO, labeled p1) or through a higher energy loose transition state to produce two radicals (H + HCO, labeled p2). (For simplicity and due to the fact that it was not part of the potential energy surface[54] used here, roaming of the H + HCO channel to produce H_2 + CO was not included here, though we expect that the effect of roaming,[55−58] which is most prevalent at energies just above the dissociation threshold, on mixture behavior would essentially serve to increase the effective energy difference between the two channels.) The most accurate treatment would be obtained from two-dimensional master equation simulations employing ab initio calculated properties for both energy and angular momentum transfer.[8] However, since such data are not yet available, the present calculations employ the common exponential-down model (eq 13) for the collisional energy transfer function and the Lennard-Jones model for the collision frequency for each collider. This treatment also affords consistency among analytical and numerical solutions to enable straightforward comparisons, permits straightforward interpretations of mixture effects, and allows compatibility with the vast majority of calculated rate constants (which use the same model).

The results below consider two-component mixtures of a weaker collider (A) and a stronger collider (B) with the properties shown in Table 1. The weaker collider (A) is

Table 1. Energy Transfer Parameters for Considered Colliders

	Z_i/Z_A	α_i (cm)$^{-1}$	$k_{0,i}/k_{0,A}$
collider A	1	$50 \times (T/298)^{0.85}$	1
collider B1	20	$50 \times (T/298)^{0.85}$	20
collider B2	1	$408 \times (T/298)^{0.85}$	20

described by Lennard-Jones parameters of σ = 3.330 Å and ϵ = 94.9 cm^{-1} and exponential-down parameters that are consistent with those used in our previous study on the single-channel HO_2 system.[41] The stronger collider (B) is considered to yield a total decomposition rate constant in the low-pressure limit, k_0, which is 20 times higher than that for A (also consistent with those considered in the single-channel study[41]) at the considered temperature (2000 K). For context, a third-body efficiency of ∼20 has been suggested for H_2O relative to Ar,[25−27,59] for example. The stronger collider is considered to have either higher Z (collider B1) or α (collider B2), to allow a more straightforward comparison of the distinct effects due to Z and α. For simplicity in terms of understanding mixture effects and assessing mixture rules, the results presented in the first three subsections of the Results and Discussion do not include tunneling (which, since H_2 + CO lies below the bottom of the CH_2O well, yields nonzero $k_p(E)$ values for all energies and results in an ill-defined low-pressure limit[60]). The effects of including tunneling (using an Eckart tunneling correction in the calculations[54]) on mixture behavior are considered in the last subsection of the Results and Discussion.

Mixture Rules. Three mixture rules are investigated in the present work as summarized in Table 2. The classic linear

Table 2. Mixture Rules for Multicomponent Pressure Dependence[a]

LMR,P	$k_{j,\mathrm{LMR,P}}(T,P,\underline{X}) = \sum_{i=1}^{M} k_{j,i}(T,P)X_i$
LMR,R	$k_{j,\mathrm{LMR,R}}(T,P,\underline{X}) = \sum_{i=1}^{M} k_{j,i}(T,R_{\mathrm{LMR}})\tilde{X}_{i,\mathrm{LMR}}$
	$R_{\mathrm{LMR}}(T,P,\underline{X}) = \frac{\sum_i k_{0,i}(T)\,X_i[M]}{k_\infty(T)}$
	$\tilde{X}_{i,\mathrm{LMR}}(T,P,\underline{X}) = \frac{k_{0,i}(T)\,X_i}{\sum_n k_{0,n}(T)\,X_n}$
NMR,R[b]	$k_{j,\mathrm{NMR,R}}(T,P,\underline{X}) = \sum_{i=1}^{M} k_{j,i}(T,R_{\mathrm{NMR}})\tilde{X}_{i,\mathrm{NMR}}$
	$R_{\mathrm{NMR}}(T,P,\underline{X}) = \frac{\sum_i f_i(T,\underline{X})\,k_{0,i}(T)\,X_i[M]}{k_\infty(T)}$
	$\tilde{X}_{i,\mathrm{NMR}}(T,P,\underline{X}) = \frac{f_i(T,\underline{X})\,k_{0,i}(T)X_i}{\sum_n f_n(T,\underline{X})\,k_{0,n}(T)X_n}$

[a]Subscripts j and i refer to the jth channel and the ith mixture component, respectively. [b]Activity coefficients, $f_i(T,\underline{X})$, in NMR,R are calculated via eq 26.

mixture rule[30] (LMR,P) approximates the rate constant of the jth channel in the mixture, $k_j(T,P,\underline{X})$, as a linear sum of the rate constants of the jth channel for each component at the given pressure, $k_{j,i}(T,P)$, weighted by their mole fractions in the mixture, X_i. Conceptually, LMR,P assumes that the contribution of each collider to the rate constant in the mixture is similar to its corresponding fractional contribution in a bath gas composed of only that collider at the given pressure. In the other two newly proposed mixture rules, the contributions of each component to the rate constant in the mixture are evaluated at the same reduced pressure, R (which, for a single-component system, is defined as $R = k_0(T)[M]/k_\infty(T)$ with the low- and high-pressure limit total decomposition rate constants, $k_0(T)$ and $k_\infty(T)$, and the total concentration, $[M]$), rather than absolute pressure, P, of the mixture. The reduced pressure, R, is a nondimensional pressure that serves as a quantitative measure of the extent of falloff from low- to high-pressure limit.[61,62] As indicated in the Results and Discussion below, the reduced pressure, R, serves as a more appropriate basis for evaluating the contributions of each component to the rate constant in the mixture for two reasons. First, rate constants for different components are much more similar when evaluated at the same reduced pressure than the same absolute pressure.[63] Second, as shown for single-channel reactions[41] and in the figures below, the quasi-steady-state distributions of the reactant during reaction in different components are much more similar at the same reduced pressure than the same absolute pressure. Since the contribution of the ith component to the rate constant in the mixture is influenced by the quasi-steady-state distribution attained in the mixture, the contribution of each component to the rate constant in the mixture is better represented by the contribution of each component evaluated at the same reduced pressure than at the same absolute pressure.

The linear mixture rule in reduced pressure (LMR,R) approximates the rate constant of the jth channel in the mixture, $k_j(T,P,\underline{X})$, as a linear sum of the rate constants of the jth channel for each component at the same reduced pressure, $k_{j,i}(T,R)$, weighted by their fractional contributions to the reduced pressure, $\tilde{X}_i$. Consistent with our other work,[42] the

DOI: 10.1021/acs.jpca.8b10581
J. Phys. Chem. A 2019, 123, 631−649

reduced pressure is based on the total decomposition rate constants, rather than the channel-specific rate constants, in the low-pressure limit. (This definition is also consistent with our previous mixture rules presented for single-channel systems[41] where this additional specification was not necessary.) While LMR,R is in fact a linear mixture rule and collapses onto LMR,P in the low-pressure limit, LMR,R generally provides a significantly more accurate representation in the intermediate falloff regime (e.g., as observed elsewhere[41,42] and below). The nonlinear mixture rule in reduced pressure (NMR,R) is similar to that for LMR,R except that the reduced pressure calculation additionally incorporates the activity coefficients for each component, which accounts for the nonlinearities in the low-pressure limit discussed above. (It is perhaps worth noting that these mixture rules, when implemented for a single-channel system, reduce to those presented in our earlier work on single-channel systems.[41])

Before applying the reduced pressure mixture rules (LMR,R and NMR,R), the rate constants for the jth decomposition channel in the ith component, $k_{j,i}(T,P)$, are mapped onto a reduced-pressure scale, $k_{j,i}(T,R_{\mathrm{LMR}})$. Thereafter, to apply LMR,R, the reduced pressure of mixture, R_{LMR}, and fractional contribution of each component to the reduced pressure of the mixture, $\tilde{X}_{i,\mathrm{LMR}}$, for a given pressure, temperature, and mixture composition are first calculated from the low- and high-pressure limit total decomposition rate constants, k_0 and k_∞, for each component and their corresponding mole fractions. Finally, the rate constants for the jth channel in the mixture, $k_{j,\mathrm{LMR,R}}$, are calculated via the summation over $k_{j,i}(T,R_{\mathrm{LMR}})$ weighted by $\tilde{X}_{i,\mathrm{LMR}}$. For NMR,R, the activity coefficients for each component, $f_i(T,\underline{X})$, are calculated prior to calculation of the reduced pressure of the mixture, R_{NMR}, and the fractional contribution of each component to the reduced pressure of the mixture, $\tilde{X}_{i,\mathrm{NMR}}$.

RESULTS AND DISCUSSION

The results and discussion below present various aspects of mixture effects for the multichannel CH_2O reaction. As discussed above in the section on Numerical Solutions of the Master Equation, the first three subsections below do not include tunneling (which results in an ill-defined low-pressure limit for this reaction[60]). The first of these subsections explores nonlinear mixture behavior in the low-pressure limit and its dependence on various characteristics of the collider mixture and reaction system. The second and third subsections, respectively, focus on the effects of different collision frequencies and different average energies transferred per collision among the colliders in the mixture across various pressures. The fourth and final subsection below explores mixture behavior when tunneling is considered in the numerical solutions.

Nonlinear Mixture Behavior in the Low-Pressure Limit. As an example of nonlinear mixture behavior in the low-pressure limit, Figure 2a presents deviations of the classic linear mixture rule (LMR,P) from solutions to the master equation across various mixture compositions of collider A and B2 (which have different average energies transferred per collision). Results are shown for both analytical and numerical solutions to the master equation, which are in very close agreement, for unimolecular reactions from CH_2O to H_2 + CO (p1), to H + HCO (p2), and to either decomposition channel (total). Similar to single-channel reaction results,[29,30] Figure 2a reveals deviations from the linear mixture rule, reaching peak

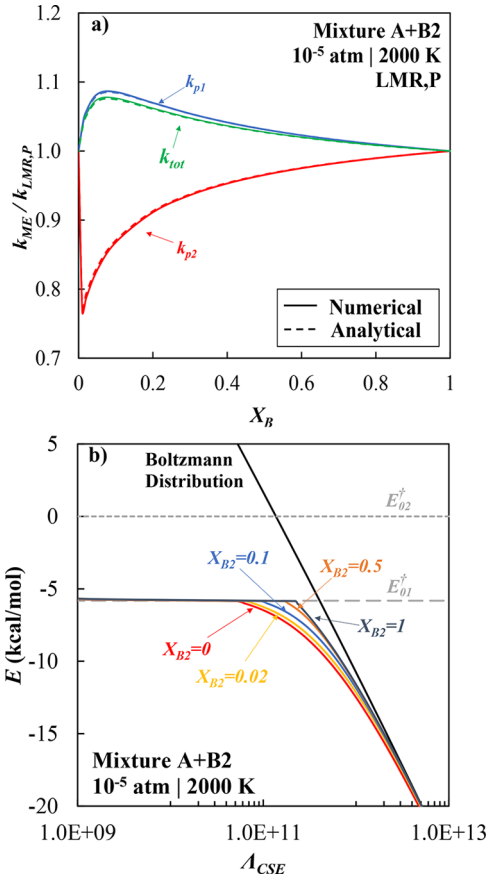

Figure 2. Nonlinear mixture behavior in the low-pressure limit for the CH_2O system (excluding tunneling) for various two-component mixtures of A and B2 (Table 1) at 2000 K: (a) comparison of numerically (solid lines) and analytically (dashed lines) calculated unimolecular rate constants and those estimated by LMR,P (Table 2); (b) chemically significant eigenvectors Λ_{CSE}.

magnitudes at lower mole fractions of the stronger collider, where the contributions of each component to the rate constant are comparable. In contrast to single-channel reactions, nonzero deviations from the linear mixture rule are not strictly positive for the channel-specific rate constants. In fact, the linear mixture rule overestimates the rate constants in the mixture for the higher energy channel (p2). Reinspection of the proof[30] that led to the conclusion for single-channel reactions that $k \geq k_{\mathrm{LMR}}$ reveals that the inequality in general applies to the slowest chemically significant eigenvalue rather than rate constants for a particular channel. Here, for a single-well multichannel reaction, the slowest (and only) chemically significant eigenvalue corresponds to the total decomposition rate constant. In fact, more generally, it can be expected that all previous trends for rate constants in mixtures for single-channel reactions should also apply to the total rate constants in mixtures for multichannel reactions.

Figure 2b shows the chemically significant eigenvector, Λ_{CSE}, for pure A, pure B2, and mixtures of A and B2. For single-well reactions, the only chemically significant eigenvector corresponds to the quasi-state distribution attained during reaction, i.e., $\Lambda_{CSE} = h(E)f(E)$. Similar to results for single-channel reactions, the quasi-steady-state energy distributions achieved in mixtures of A and B2 are different than those achieved for either of the two pure components, where the quasi-steady-state population near the lowest decomposition threshold is

DOI: 10.1021/acs.jpca.8b10581
J. Phys. Chem. A 2019, 123, 631−649

preferentially depleted for weaker colliders (as discussed elsewhere[44]). Consistent with eq 16, the quasi-steady-state population at energies just below the dissociation threshold is higher for pure B2, which has a higher average energy transferred per collision, than for pure A. (Conceptually, weak collisions preferentially deplete the states just below the dissociation threshold because they can only excite reactive complexes above the decomposition threshold from reactant energies just below the lowest decomposition threshold; in contrast, infinitely strong colliders can excite reactive complexes above the decomposition threshold equally from all reactant energies and so deplete all states equally, such that the quasi-steady-state energy distribution below the decomposition threshold is the same as the Boltzmann distribution.) Accordingly, the quasi-steady-state population at energies just below the dissociation threshold in the mixture will be higher than that for pure A but lower than that for pure B.

As indicated by supra-unity activity coefficients for A and subunity activity coefficients for B2, A serves to weaken the ability of B2 to induce collisions above the dissociation threshold to yield reaction by depleting near-threshold populations and, likewise, B2 serves to strengthen the ability of A to induce collisions above the dissociation threshold by maintaining higher near-threshold populations. Since each component has different fractional contributions to rate constants for different channels, these interactions can have different effects for different channels (even though the activity coefficients are channel-independent). In particular, this can lead to negative deviations from the linear mixture rule for rate constants to the higher energy channel, for which B2 is almost exclusively responsible (consistent with expectations based on the fact that $k_{02}/k_0 \sim \exp(-(E_{02}^{\dagger} - E_{01}^{\dagger})/\alpha)$) for pure weak components[43]). For this case, A contributes minimally to the higher energy channel but serves to reduce the effectiveness of B2 in inducing collisions above $E_{02}^{\dagger}$ by depleting the states just below the dissociation threshold (similar to increasing the difference between $E_{02}^{\dagger}$ and $E_{01}^{\dagger}$), thus requiring collisions transferring more energy to excite reactants above $E_{02}^{\dagger}$.

To explore trends with characteristics of the collider mixture and reaction system, the maximum deviations of LMR,P for channel-specific rate constants in the low-pressure limit are quantified in Figure 3 as functions of various collider mixture and system properties. Again, results are shown for both analytical and numerical solutions to the master equation. The small difference (<5%) between analytical and numerical solutions across a wide range of collider and reaction system characteristics suggest general applicability of the activity coefficients in representing nonlinear mixture behavior in low-pressure limit (for use in NMR,R for example). From panels a–d of Figure 3, it is also clear that in the low-pressure limit:

(a) The linear mixture rule is exact for mixtures composed of colliders with differing collision frequencies but the same average energy transferred per collision, consistent with conclusions based on the analytical solutions of the master equation above.

(b) Differences in average energies transferred per collision among colliders have significant influences on deviations of LMR,P for all channels. Consistent with previous work on single-channel reactions, the deviations of LMR,P for the total rate constant are larger for larger differences in the average energies transferred per collision between the two components. Deviations of LMR,P for rate constants for the lower energy channel (p1), which dominates the total rate constant, are similar to those for the total rate constant though are slightly larger, given that A, whose activity coefficient is supra-unity, has a larger fractional contribution to k_{p1} than to k_0. By contrast, deviations of LMR,P for rate constants for the higher

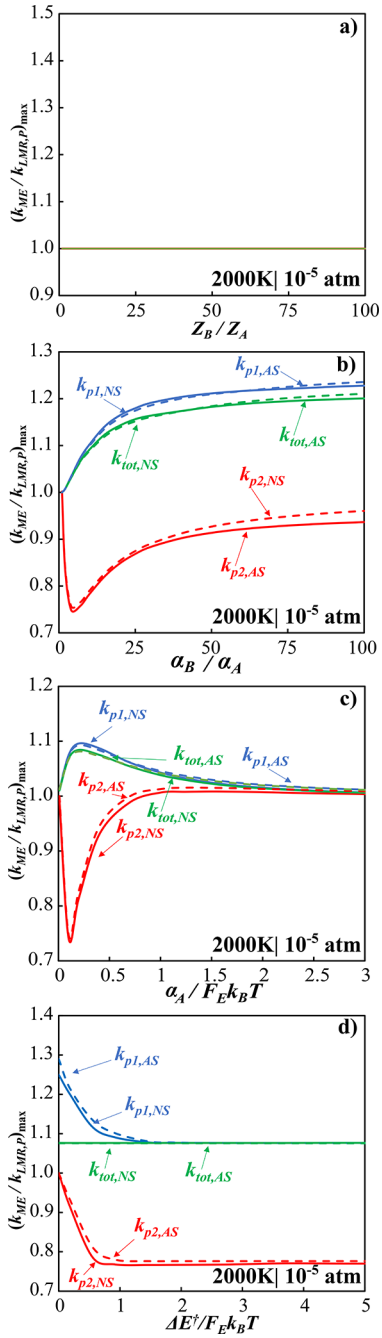

Figure 3. Deviations of LMR,P from numerical solutions (solid lines) and analytical solutions (dashed lines) of the master equation for channel-specific rate constants in the low-pressure limit for the CH_2O system (excluding tunneling) at 2000 K as a function of (a) ratio of collision frequencies of A and B, Z_B/Z_A (for $\alpha_A = \alpha_B = 50(T/298\ K)^{0.85}\ cm^{-1}$), (b) ratio of average energies transferred per down collision for A and B, α_B/α_A (for $\alpha_A = 50(T/298\ K)^{0.85}\ cm^{-1}$), (c) ratio of average energies transferred per down collision to the weighted Boltzmann factor, $\alpha_A/F_E k_B T$ (for $\alpha_B/\alpha_A = 8$), and (d) ratio of differences in decomposition threshold energies for each channel, $\Delta E^{\dagger} = E_{02}^{\dagger} - E_{01}^{\dagger}$, to the weighted Boltzmann factor, $\Delta E^{\dagger}/F_E k_B T$ (for fixed $E_{01}^{\dagger}$, $\alpha_A = 50(T/298\ K)^{0.85}\ cm^{-1}$, and $\alpha_B = 408(T/298\ K)^{0.85}\ cm^{-1}$).

DOI: 10.1021/acs.jpca.8b10581
J. Phys. Chem. A 2019, 123, 631–649

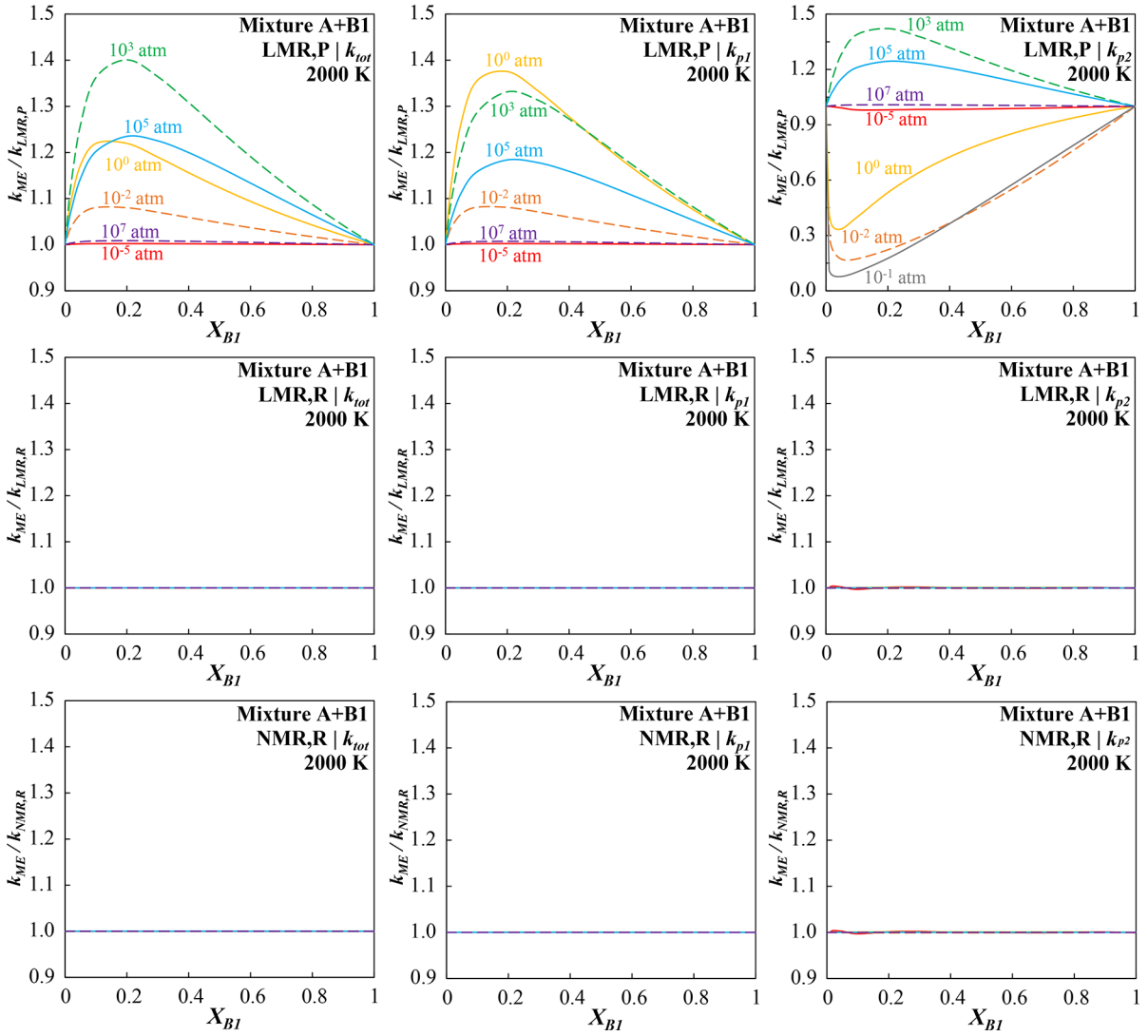

Figure 4. Comparisons of numerically calculated unimolecular rate constants and those estimated by various mixture rules (Table 2) at 2000 K for the CH_2O system (excluding tunneling) across various pressures for various two-component mixtures of A and B1 (Table 1). Different mixture rules are plotted in different rows: LMR,P (first row); LMR,R (second row); NMR,R (third row). Different channels are plotted in different columns: total reaction, k_{tot} (first column); H_2 + CO, k_{p1} (second column); H + HCO, k_{p2} (third column).

energy channel (p2) exhibit a nonmonotonic dependence on α_B/α_A where the magnitude of the deviations first grow with increasing α_B/α_A though eventually decay with increasing α_B/α_A as B approaches the strong collision limit ($\alpha_B/F_E k_B T \to \infty$, for fixed α_A). Consequently, as per eq 26, the activity coefficient f_B for B, which dominates the rate constant to the higher channel, approaches unity. Conceptually, as the stronger collider B approaches the strong-collision limit, the ability of B to excite reactive complexes above the higher decomposition threshold, $E_{02}^{\dagger}$, is no longer hampered by the fact that collisions by the weaker collider A have preferentially depleted the states near the lowest decomposition threshold, $E_{01}^{\dagger}$.

(c) The maximum deviations of LMR,P have a nonmonotonic dependence on the ratio of the average energy transferred per down collision of A to the weighted Boltzmann factor, $\alpha_A/F_E k_B T$ (with fixed $\alpha_B/\alpha_A = 8$), for all channels. The maximum deviations peak at moderate $\alpha_A/F_E k_B T$ ratios (near ~0.1 in this case) and then approach zero for all channels as $\alpha_A/F_E k_B T \to 0$ (the weak collision limit) and $\alpha_A/F_E k_B T \to \infty$ (the strong collision limit). In both limits, the quasi-steady-state distribution below the decomposition threshold is independent of collider properties and is thus same for A and B, with $h(E) = 1 - \exp[-(E_{01}^{\dagger} - E)/F_E k_B T]$ in the weak collision limit and $h(E) = 1$ in the strong collision limit, as per eq 16, as discussed above.

(d) The maximum deviations of LMR,P for only the channel-specific rate constants depend on the difference in decomposition thresholds for each channel, $\Delta E^{\dagger} = E_{02}^{\dagger} - E_{01}^{\dagger}$ (at fixed $E_{01}^{\dagger}$), whereas the maximum deviations for the total rate constant do not. For small differences between the decomposition thresholds, $\Delta E^{\dagger}$, maximum deviations of LMR,P for p1, which proceeds through a tight transition state, are higher than those for the total rate constant since the fractional contribution of A, whose activity coefficient is supra-unity, to k_{p1} is higher than that to k_0 (or k_{p2}). For larger differences between the decomposition thresholds, $\Delta E^{\dagger}$, k_0 is dominated by k_{p1} such that the deviations become similar for k_0 and k_{p1}. For the p2 channel, the maximum deviations monotonically decrease to subunity values with increasing differences in the decomposition thresholds, $\Delta E^{\dagger}$, eventually

DOI: 10.1021/acs.jpca.8b10581
J. Phys. Chem. A 2019, 123, 631−649

reaching a plateau at larger $\Delta E^{\dagger}$ with a value near that of the activity coefficient for B (which dominates k_{p2} at the mole fractions of maximum deviation) as $X_B \rightarrow 0$.

Effect of Differing Collision Frequencies across Various Pressures. Figures 4–6 show results for various mixtures of A and B1, which have the same α but different Z_i (Table 1). Comparisons of rate constants numerically calculated from the master equation and those estimated by various mixture rules in Table 2 are shown for unimolecular reactions from CH_2O to H_2 + CO (p1), H + HCO (p2), and to either decomposition channel (total) in Figure 4. Quasi-steady-state energy distributions are shown in Figure 5.

Because colliders with different Z_i but the same α yield master equations (cf. eq 1) that differ only in terms of the collision rate, $Z_i[M_i]$, the quasi-steady-state distribution and the rate constant for any channel are identical for B1 (which has a collision frequency 20 times higher than that for A) at some pressure to A at a 20 times higher pressure. Therefore, when evaluated at the same reduced pressure, all results for any mixture of A and B1 are identical, as observed in Figure 5;

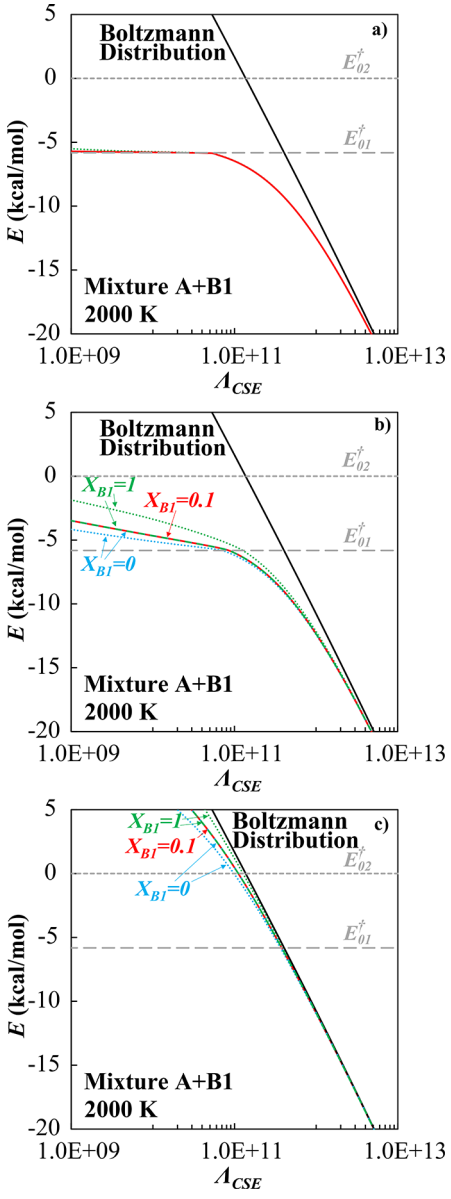

Figure 5. Chemically significant eigenvectors Λ_{CSE} (corresponding to the quasi-steady-state distribution during reaction) at 2000 K for the CH_2O system (excluding tunneling) for various two-component mixtures of A + B1 for (a) the low-pressure limit ($P = 10^{-5}$ atm, $R \approx 1.7 \times 10^{-8}$), (b) lower intermediate pressures ($P = 10^{-2}$ atm, $R \approx 1.7 \times 10^{-5}$) that yield maximum (negative) LMR,P deviation for k_{p2}, and (c) higher intermediate pressures ($P = 10^{3}$ atm, $R \approx 1.7$) that yield maximum positive LMR,P deviation for k_{p2}. The solid line denotes Λ_{CSE} for the mixture, dotted lines denote Λ_{CSE} for pure components evaluated at the same P as the mixture, and dashed lines (which overlap with the solid line) denote Λ_{CSE} evaluated at the same R as the mixture.

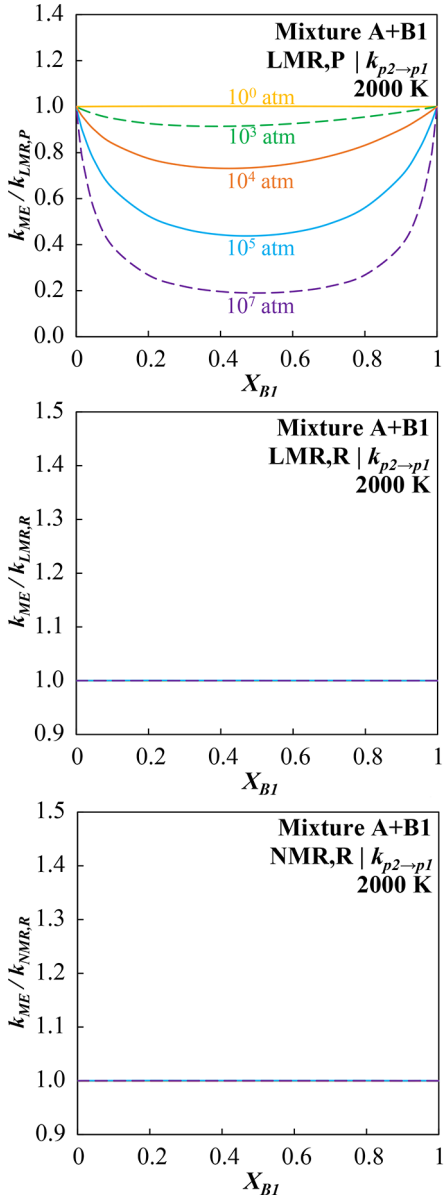

Figure 6. Comparisons of numerically calculated bimolecular rate constants ($k_{p2\rightarrow p1}$) from H + HCO (p2) to H_2 + CO (p1) and those estimated by various mixture rules (Table 2) at 2000 K for the CH_2O system (excluding tunneling) across various pressures for various two-component mixtures of A and B1 (Table 1). Different mixture rules are plotted in different rows: LMR,P (first row); LMR,R (second row); NMR,R (third row). Deviations for various mixture rules for other bimolecular channels (i.e., total bimolecular reaction, $k_{bi,tot}$, and H + HCO to CH_2O, $k_{p2\rightarrow w}$) are included in the Supporting Information.

DOI: 10.1021/acs.jpca.8b10581
J. Phys. Chem. A 2019, 123, 631–649

similarly, LMR,R and NMR,R are exact at all pressures and mole fractions, as observed in Figures 4 and 6.

By contrast, quasi-steady-state distributions and rate constants for A, B1, and their mixtures are considerably different when evaluated at the same absolute pressure. Likewise, as demonstrated in Figure 4, while the classic linear mixture rule (LMR,P) is exact in the low-pressure limit (for mixtures of bath gases with the same α, as discussed above) and the high-pressure limit (which is pressure- and composition-independent for thermally activated reactions), LMR,P differs substantially from master equation calculations in the intermediate falloff regime, with errors reaching an order of magnitude for some channels.

The deviations are asymmetric with respect to X_{B1} and peak at lower X_{B1} values, where the contributions of each component to the overall reaction are comparable. Across the entire intermediate falloff regime, LMR,P always underestimates k_{p1} and k_{tot}, predicting rate constants that are too low by ~40%. For k_{p2}, LMR,P overestimates k_{p2} at lower intermediate pressures, predicting rate constants that are too high by a factor of ~10, and then underestimates k_{p2} at higher intermediate pressures, predicting rate constants that are too low by ~40%. While the maximum deviations of LMR,P of ~40% for k_{p1} and k_{tot} are of comparable magnitude to those observed previously for single-channel reactions,[41] the maximum deviations of LMR,P for k_{p2} are considerably higher than those observed for single-channel reactions.

Interestingly, while LMR,P strictly underestimates rate constants for the total reaction,[30] LMR,P can underestimate or overestimate channel-specific rate constants depending on the channel and the pressure. The direction of the deviations can be rationalized on the basis of the quasi-steady-state distributions attained in the pure components and mixtures as well as how rate constants scale with pressure in different pressure regimes.

As shown in Figure 5a, in the low-pressure limit, where collision rates are much less than decomposition rates, collisions are not able to sustain finite populations above the lowest dissociation threshold due to rapid depletion of these states by decomposition. Consequently, all collisions that excite reactants above $E_{01}^{\dagger}$ result in reaction, such that the rate of collisions to excite CH_2O above $E_{0j}^{\dagger}$ is the rate-limiting step for each jth channel. The rate of collisions to excite CH_2O above $E_{0j}^{\dagger}$ is proportional to both the total collision rate, which always scales linearly with P, and the probability that a given collision will excite CH_2O above $E_{0j}^{\dagger}$, which is independent of P in the low-pressure limit since Λ_{CSE} is independent of P. Consequently, k scales linearly with P. Similarly, since A and B1 yield the same Λ_{CSE} in the low-pressure limit, the likelihood that collision with A (or B1) will excite CH_2O above $E_{0j}^{\dagger}$ is the same in the mixture as it is for pure A (or B1). Therefore, as indicated in Figure 4, there is no deviation of LMR,P for any channel in the low-pressure limit.

As the pressure increases, and concomitantly the collision rate increases, collisions are increasingly able to compete with decomposition and are able to sustain substantial populations at higher energies, as shown in Figure 5b,c. At all pressures beyond the low-pressure limit, not all complexes excited above $E_{01}^{\dagger}$ by collisions lead to reaction (given that down collisions can remove CH_2O at $E > E_{01}^{\dagger}$ in addition to decomposition). Consequently, the rate of collisions to excite CH_2O above $E_{01}^{\dagger}$ is no longer the only rate-limiting step for the total reaction or the reaction to H_2 + CO (p1). As a result, both k_{tot} and k_{p1} scale less than linearly with P. Evaluating the quasi-steady-state distribution, k_{tot}, and k_{p1} for pure B1 at the same P rather than same R as the mixture serves to overestimate the population of CH_2O above $E_{01}^{\dagger}$ and the associated decrease in the effectiveness of collisions by B1 in inducing total reaction or reaction to H_2 + CO (p1). The contribution of B1, which is dominant for $X_B \gtrsim 0.05$, to k_{tot} and k_{p1} in the mixture, if evaluated at the same P, is underestimated relative to its predicted contribution if evaluated at the same R. Therefore, as indicated in Figure 4, LMR,P underestimates k_{tot} and k_{p1} in the mixture for intermediate pressures.

At lower intermediate pressures, as shown in Figure 5b, there are substantial populations only for states with $E < E_{02}^{\dagger}$, whereas states with $E > E_{02}^{\dagger}$ are still completely depleted by reactions. For this range of pressures, all complexes excited above $E_{02}^{\dagger}$ by collisions undergo decomposition (via either channel). Consequently, the rate of collisions to excite CH_2O above $E_{02}^{\dagger}$ is still the rate-limiting step. The rate of collisions to excite CH_2O above $E_{02}^{\dagger}$ is proportional to both the total collision rate, which always scales linearly with P, and the probability that a given collision will excite CH_2O above $E_{02}^{\dagger}$, which also increases with P (since higher collision rates can sustain finite populations at energies closer to $E_{02}^{\dagger}$). In this pressure regime, k_{p2} has a greater than linear dependence on P, as discussed elsewhere.[64,65] Evaluating the quasi-steady-state distribution and k_{p2} for pure B1 at the same P (10^{-2} atm), rather than the same R (1.7×10^{-4}), as for the mixture serves to overestimate the CH_2O population above $E_{01}^{\dagger}$ and the associated increased likelihood of a given collision by B1 exciting CH_2O above $E_{02}^{\dagger}$. The contribution of B1, which is dominant for $X_B \gtrsim 0.05$, to k_{p2} in the mixture, if evaluated at the same P, is overestimated relative to its predicted contribution if evaluated at the same R. Therfore, as indicated in Figure 4, LMR,P overestimates k_{p2} in the mixture at this pressure.

At higher intermediate pressures, collisions are able to sustain finite populations even above $E_{02}^{\dagger}$, as shown in Figure 5c. At these and higher pressures, not all complexes excited above $E_{02}^{\dagger}$ by collisions lead to reaction (given that down collisions can remove CH_2O at $E > E_{02}^{\dagger}$ in addition to decomposition). Consequently, the rate of collisions to excite CH_2O above $E_{02}^{\dagger}$ is no longer the only rate-limiting step for the reaction to H + HCO (p2). As a result, k_{p2} has a less than linear dependence on P. Evaluating the quasi-steady-state distribution and k_{p2} for pure B1 at the same P rather than same R as the mixture serves to overestimate the population of CH_2O above $E_{02}^{\dagger}$ and the associated decrease in the effectiveness of collisions of B1 in inducing reaction to H + HCO (p2). The contribution of B1, which is dominant for $X_B \gtrsim 0.05$, to k_{p2} in the mixture, if evaluated at the same P, is underestimated relative to its predicted contribution if evaluated at the same R. As indicated in Figure 4, LMR,P underestimates k_{p2} in the mixture for higher intermediate pressures.

In the high-pressure limit, where collision rates are much larger than decomposition rates, collisions are able to maintain Boltzmann populations at all energies. Collisions are no longer rate-limiting at all. Consequently, all rate constants are independent of P and mixture composition.

Comparisons of rate constants numerically calculated from the master equation and those estimated by various mixture rules in Table 2 are shown in Figure 6 for bimolecular reactions from H + HCO proceeding via chemically activated

DOI: 10.1021/acs.jpca.8b10581
J. Phys. Chem. A 2019, 123, 631−649

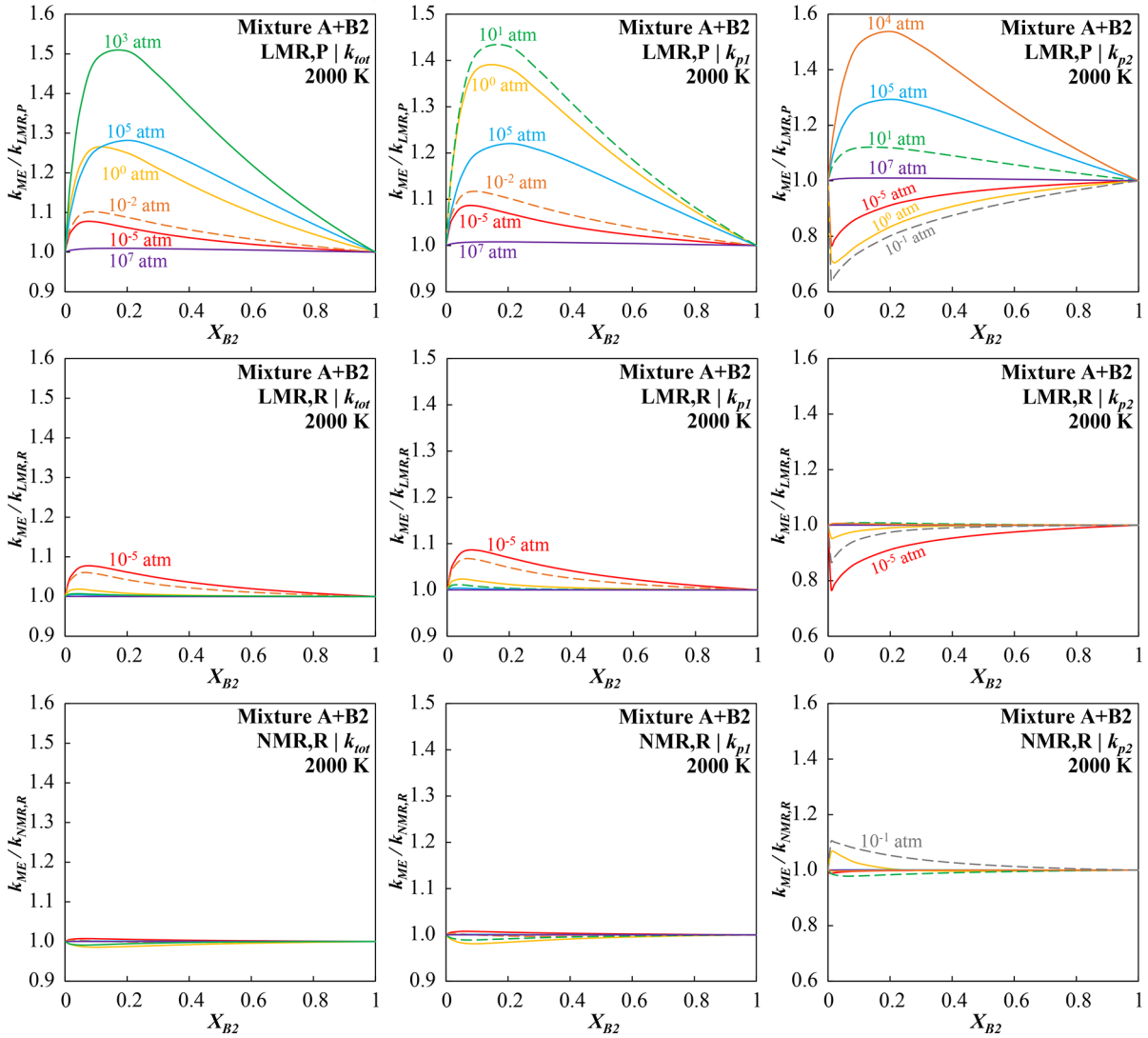

Figure 7. Comparisons of numerically calculated unimolecular rate constants and those estimated by various mixture rules (Table 2) at 2000 K for the CH_2O system (excluding tunneling) across various pressures for various two-component mixtures of A and B2 (Table 1). Different mixture rules are plotted in different rows: LMR,P (first row); LMR,R (second row); NMR,R (third row). Different channels are plotted in different columns: total reaction, k_{tot} (first column); H_2 + CO, k_{p1} (second column); H + HCO, k_{p2} (third column).

CH_2O to form H_2 + CO (with rate constant $k_{p2\rightarrow p1}$). (Note that even for the bimolecular reactions the total unimolecular rate constant is still used for calculating R for the mixture in LMR,R and NMR,R.) While LMR,P is exact in the low-pressure limit for $k_{p2\rightarrow p1}$ (where $k_{p2\rightarrow p1}$ is pressure- and composition-independent), $k_{p2\rightarrow p1}$ estimated by LMR,P increasingly differs from that calculated numerically as pressure increases. At pressures above the low-pressure limit, a finite fraction of the chemically activated CH_2O are stabilized to thermal CH_2O instead of promptly decomposing. This fraction grows with increasing P, such that $k_{p2\rightarrow p1}$ decreases with P, scaling with $1/P$ in the high-pressure limit. With increasing pressure, LMR,P increasingly overestimates $k_{p2\rightarrow p1}$ in the mixture. By contrast, as observed for unimolecular decomposition channels, Figure 6 shows that LMR,R and NMR,R are exact for the ("well-skipping") chemically activated channel, $k_{p2\rightarrow p1}$, across the entire pressure range for mixtures of A and B1, suggesting that summing the contributions of mixture components evaluated at the same R (calculated on the basis of the total unimolecular rate constants, cf. Table 2) is also a useful basis for evaluating bimolecular channels (including "well-skipping" chemically activated channels) in LMR,R and NMR,R.

Effect of Differing Average Energies Transferred per Collision across Various Pressures. Figures 7–9 shows results for various mixtures of A and B2, which have the same Z but different α_i (Table 1). Comparisons of rate constants numerically calculated by the master equation and those estimated by various mixture rules in Table 2 are shown for unimolecular reactions from CH_2O to H_2 + CO (p1), H + HCO (p2), and to either decomposition channel (total) in Figure 7. Quasi-steady-state energy distributions are shown in Figure 8. The results obtained for mixtures of A and B2 are generally similar to those for mixtures of A and B1 with the important difference that nonlinearities arise even in the low-pressure limit for mixtures of A and B2, which have different α (as discussed above).

Specifically, because colliders with different α_i but the same Z yield master equations (cf. eq 1) that differ in terms of their collisional energy transfer probability function, $P_i(E',E)$ (eq

DOI: 10.1021/acs.jpca.8b10581
J. Phys. Chem. A 2019, 123, 631–649

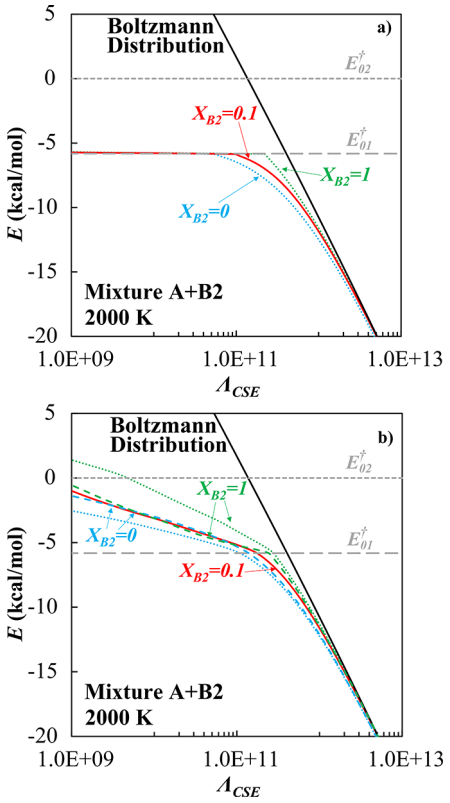

Figure 8. Chemically significant eigenvectors Λ_{CSE} (corresponding to the quasi-steady-state distribution during reaction) at 2000 K for the CH_2O system (excluding tunneling) for various two-component mixtures of A and B2: (a) low-pressure limit ($P = 10^{-5}$ atm, $R \approx 1.9 \times 10^{-8}$); (b) lower intermediate pressures ($P = 10^{-1}$ atm, $R \approx 1.9 \times 10^{-4}$) that yield maximum LMR,P deviation for k_{p2}.

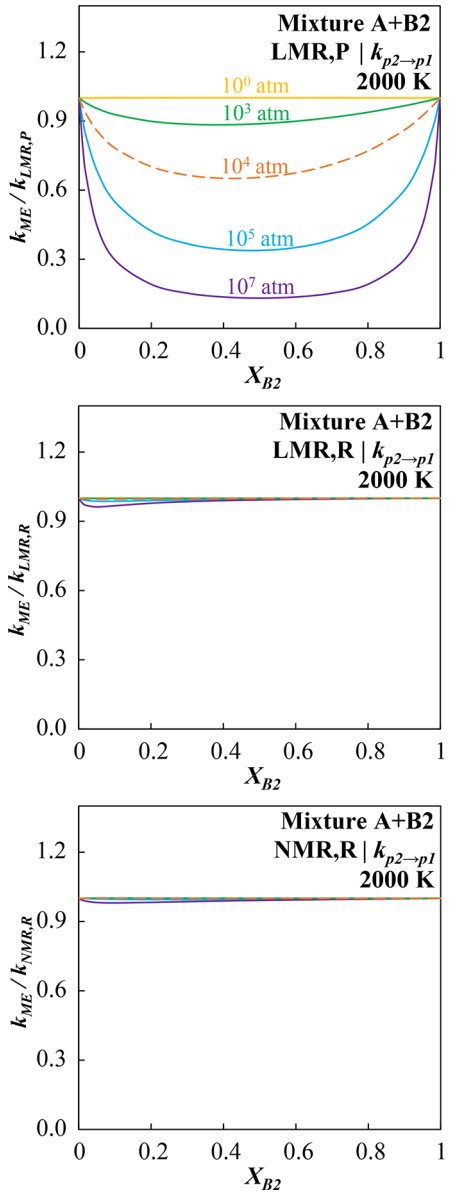

Figure 9. Comparisons of numerically calculated bimolecular rate constants ($k_{p2\rightarrow p1}$) from H + HCO (p2) to H_2 + CO (p1) and those estimated by various mixture rules (Table 2) at 2000 K for the CH_2O system (excluding tunneling) across various pressures for various two-component mixtures of A and B2 (Table 1). Different mixture rules are plotted in different columns: LMR,P (first column); LMR,R (second column); NMR,R (third column). Deviations for various mixture rules for other bimolecular channels (i.e., total bimolecular reaction, $k_{bi,tot}$ and H + HCO to CH_2O, $k_{p2\rightarrow w}$) are included in the Supporting Information.

10), the quasi-steady-state distribution and rate constants for B2 are not identical to those for A at any pressure below the high-pressure limit. Therefore, neither LMR,P nor LMR,R is exact for any pressure below the high-pressure limit.

However, the quasi-steady-state distributions for A, B2, and their mixtures are much more similar when evaluated at the same reduced pressure, R, than at the same absolute pressure, P (Figure 8). Likewise, as shown in Figure 7, deviations of LMR,R (of up to ~30%) are considerably lower than those of LMR,P (of up to ~50%) and strictly decrease with increasing pressure. Furthermore, deviations of NMR,R, which accounts for nonlinearities in the low-pressure limit via the activity coefficients f_i from the analytical solutions above, are even lower (up to 8%) and peak at intermediate pressures.

It is also worth emphasizing the importance of using the total unimolecular rate constant, instead of the channel-specific rate constants, for defining the reduced pressure R used for the reduced-pressure-based mixture rules for multichannel systems—use of the channel-specific rate constants instead of the total unimolecular rate constant for calculating R results in deviations from numerically calculated rate constants reaching a factor of 4.

Comparisons of rate constants numerically calculated by the master equation and those estimated by various mixture rules (Table 2) are shown in Figure 9 for bimolecular reactions from H + HCO proceeding via chemically activated CH_2O to form H_2 + CO (with rate constant $k_{p2\rightarrow p1}$). (Note again that even for the bimolecular reactions the total unimolecular rate constant is still used for calculating R for the mixture in LMR,R and NMR,R.) Similar to observations for mixtures of A and B1, with increasing pressure above the low-pressure limit, LMR,P increasingly overestimates $k_{p2\rightarrow p1}$ in mixtures of A and B2. While Figure 6 shows that LMR,R and NMR,R are not quite exact for ("well-skipping") chemically activated channels, $k_{p2\rightarrow p1}$, in mixtures of A and B2 (in contrast to mixtures of A and B1), deviations of LMR,R and NMR,R are relatively minimal (<3%), similarly suggesting that summing the rate constant contributions in each mixture component evaluated at the same R (calculated on the basis of the total unimolecular

DOI: 10.1021/acs.jpca.8b10581
J. Phys. Chem. A 2019, 123, 631−649

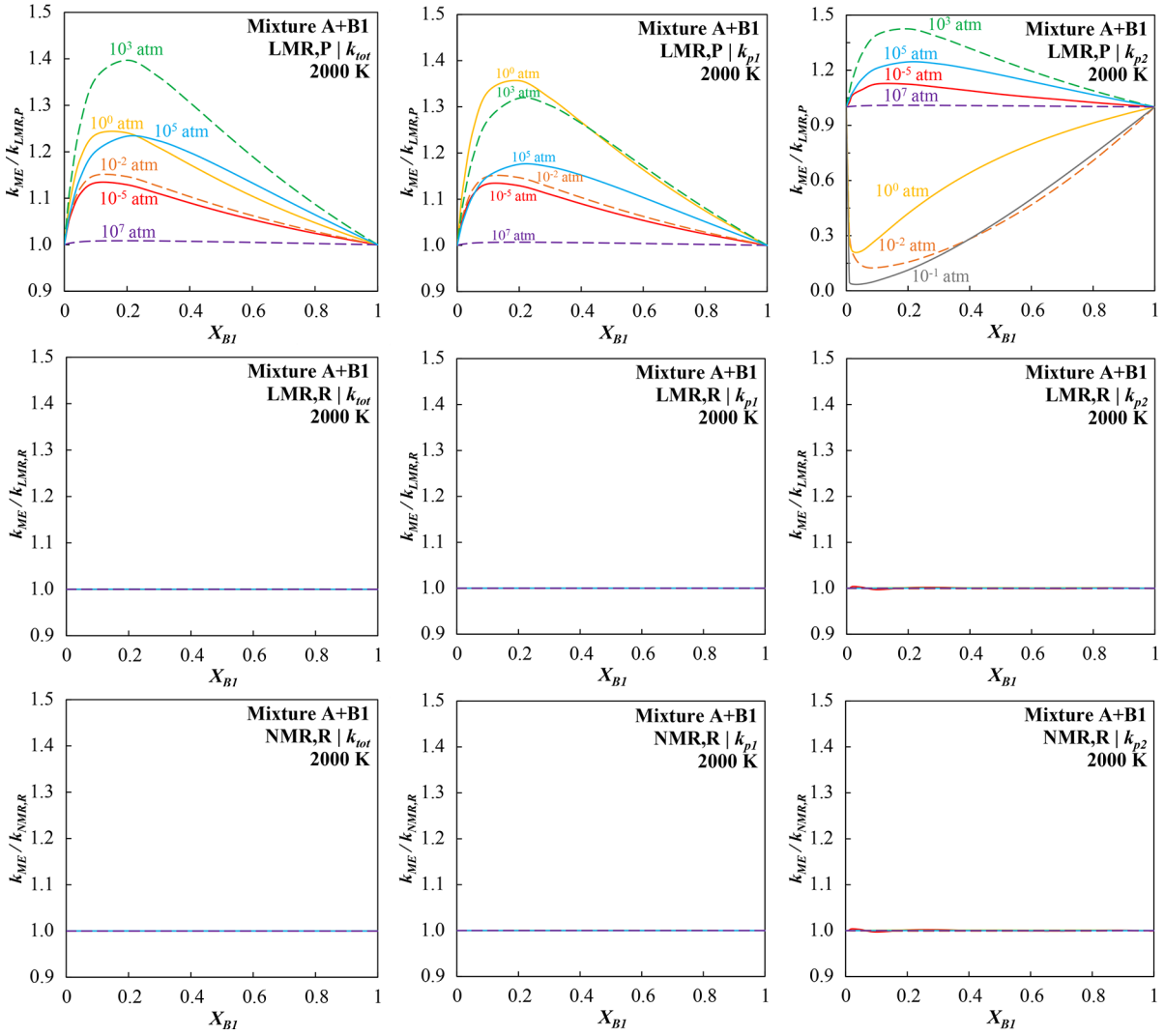

Figure 10. Comparisons of numerically calculated unimolecular rate constants and those estimated by various mixture rules (Table 2) at 2000 K for the CH_2O system (including tunneling) across various pressures for various two-component mixtures of A and B1 (Table 1). Different mixture rules are plotted in different rows: LMR,P (first row); LMR,R (second row); NMR,R (third row). Different channels are plotted in different columns: total reaction, k_{tot} (first column); H_2 + CO, k_{p1} (second column); H + HCO, k_{p2} (third column).

rate constants even including activity coefficients derived for unimolecular reactions in the low-pressure limit) is also a useful basis for evaluating bimolecular channels (including "well-skipping" chemically activated channels) in LMR,R and NMR,R.

Effect of Tunneling across Various Pressures. The effect of quantum tunneling on representing the multicomponent mixture effects were also investigated under the same conditions as the previous sections. For reaction channels with intrinsic potential barriers (as for CH_2O = H_2 + CO), tunneling produces nonzero $k_p(E)$ values even below the saddle point on potential energy surface. In the case of the CH_2O = H_2 + CO channel, since H_2 + CO (p1) lies below the bottom of the CH_2O well, $k_p(E)$ is nonzero for all energies, resulting in a rate constant that "falls off forever" with pressure,[60] such that there is no well-defined low-pressure limit. Without a well-defined low-pressure limit, the reduced pressure (as required by the better-performing mixture rules, LMR,R and NMR,R) is also not well-defined in the usual sense. However, there is reason to believe that evaluating rate constants at some "effective reduced pressure" may still yield better predictions for mixtures than evaluating rate constants at the absolute pressure P. In the results shown below, the effective reduced pressure is based on a total effective low-pressure-limit unimolecular rate constant, $k_{0,eff}$ = $k_{tot}/[M]$, calculated from the total unimolecular rate constants at 10^{-6} atm (as if it were a pressure where the reaction was actually in the low-pressure limit); similarly, activity coefficients derived in the low-pressure limit above are still used for results shown for NMR,R.

In general, the results for the calculations that consider tunneling are qualitatively similar to those where tunneling was excluded, provided that one recognizes that the reaction is in the intermediate falloff regime even at the lowest pressures.

Comparisons of the various mixture rules of Table 2 against numerical calculations are shown in Figure 10 for unimolecular reactions and in Figure 11 for bimolecular reactions for a mixture of A + B1, which differ only in their Z_i. Overall, deviations of LMR,P exhibit a pressure dependence (both trends and magnitude) similar to that observed in calculations where tunneling was not included. However, since the reaction is in the intermediate falloff regime even at the lowest

DOI: 10.1021/acs.jpca.8b10581
J. Phys. Chem. A 2019, 123, 631−649

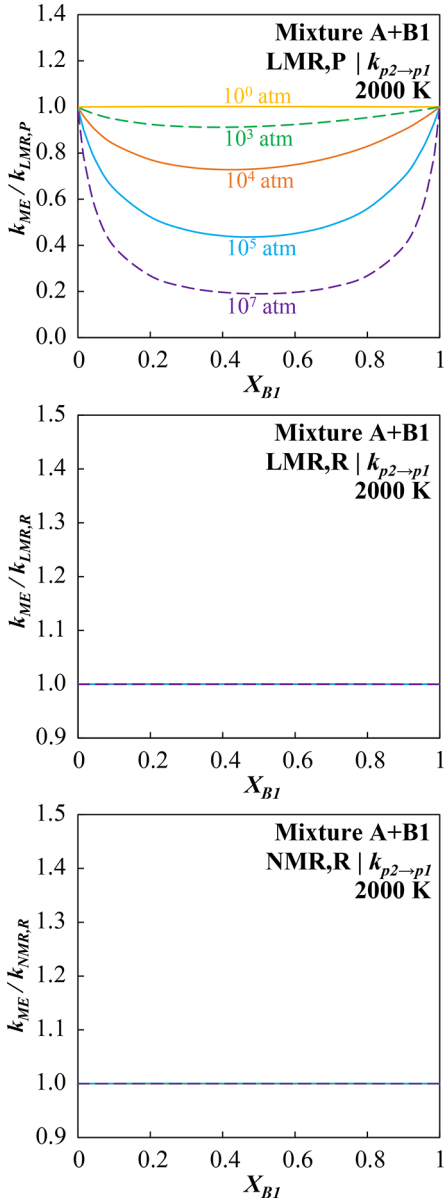

Figure 11. Comparisons of numerically calculated bimolecular rate constants ($k_{p2\rightarrow p1}$) from H + HCO (p2) to H_2 + CO (p1) and those estimated by various mixture rules (Table 2) at 2000 K for the CH_2O system (including tunneling) across various pressures for various two-component mixtures of A and B1 (Table 1). Different mixture rules are plotted in different rows: LMR,P (first row); LMR,R (second row); NMR,R (third row). Deviations for various mixture rules for other bimolecular channels (i.e., total bimolecular reaction, $k_{bi,tot}$, and H + HCO to CH_2O, $k_{p2\rightarrow w}$) are included in the Supporting Information.

pressures, LMR,P differs from the numerical calculations (by 15%) even at the lowest pressure. Additionally, the maximum deviations when tunneling is included are higher, reaching a factor of ~50, than those without tunneling. By contrast, for reasons similar to those discussed in the section above for mixtures of A + B1, LMR,R and NMR,R are exact for all mole fractions and pressures, indicating that use of an "effective reduced pressure" is still a useful basis for evaluating rate constants in mixtures for reactions without well-defined low-pressure limits.

Comparisons of the various mixture rules of Table 2 against numerical calculations are shown in Figure 12 for unimolecular reactions and in Figure 13 for bimolecular reactions for a mixture of A + B2, which differ only in their α_i. Overall, deviations of LMR,P exhibit trends and magnitudes (reaching ~60%) similar to those observed in calculations excluding tunneling. However, since the reaction is in the intermediate falloff regime (where deviations of LMR,P are largest), the deviations of LMR,P are slightly larger (~40% instead of ~30%) at the lowest pressure. By contrast, deviations of LMR,R and NMR,R are much smaller (below 10%) across the entire pressure range. In fact, deviations of LMR,R are smaller than those observed for calculations excluding tunneling (where deviations reached ~30% in the low-pressure limit and monotonically decreased in magnitude through the intermediate falloff regime).

Altogether, the results above suggest that use of an "effective reduced pressure" within LMR,R and NMR,R can still provide a reasonably accurate means of representing mixture dependence. We expect that such a result may be useful either for reactions that do not have a well-defined low-pressure limit (like CH_2O decomposition) or for reactions where low-pressure limit data are not available.

CONCLUSIONS

The master equation was solved analytically and numerically for a multichannel reaction in a bath gas mixture to explore mixture behavior and mixture rules for multichannel reactions. The analytical solutions extend previous derivations of single-channel reactions in a two-component mixture to an *N*-channel reaction in an *M*-component mixture. The analytical solutions agree very well with numerical solutions for the H_2 + CO = CH_2O = H + HCO reaction as a case study.

With regard to general trends for multichannel reactions, the results indicate the following in the low-pressure limit:

(1) Similar to rate constants for single-channel reactions, rate constants for multichannel reaction systems in general follow a nonlinear, rather than linear, mixture rule (eqs 22, 25, and 26). The origin of this nonlinearity is related to the fact that the quasi-steady-state distribution in the mixture may differ from that in the pure bath gases, such that each mixture component interacts with a different distribution of reactants in the mixture than when pure. This nonlinear mixture rule is found to approach a linear mixture rule in the following special cases, where the quasi-steady-state distribution below the lowest decomposition threshold is the same in the mixture and its components when pure: (a) all components share the same α (but may differ in Z_i); (b) the strong collision limit (all $\alpha_i/F_E k_B T \gg 1$); (c) the weak collision limit (all $\alpha_i/F_E k_B T \ll 1$).

(2) Similar to single-channel reactions, the nonlinear interactions among mixture components can be well represented through activity coefficients, f_i, which describe how the contribution of each component is affected by the presence of the other components (eq 26). Interestingly, in the multichannel case, the results indicate that the activity coefficients are the same for every channel (at least for the energy transfer model used in the present study). However, the effect of these activity coefficients on the rate constant may be different for each channel, given that different components may have different fractional contributions to the rate constants for each channel.

(3) In contrast to single-channel reactions, the linear mixture rule does not strictly underestimate the rate constant

DOI: 10.1021/acs.jpca.8b10581
J. Phys. Chem. A 2019, 123, 631−649

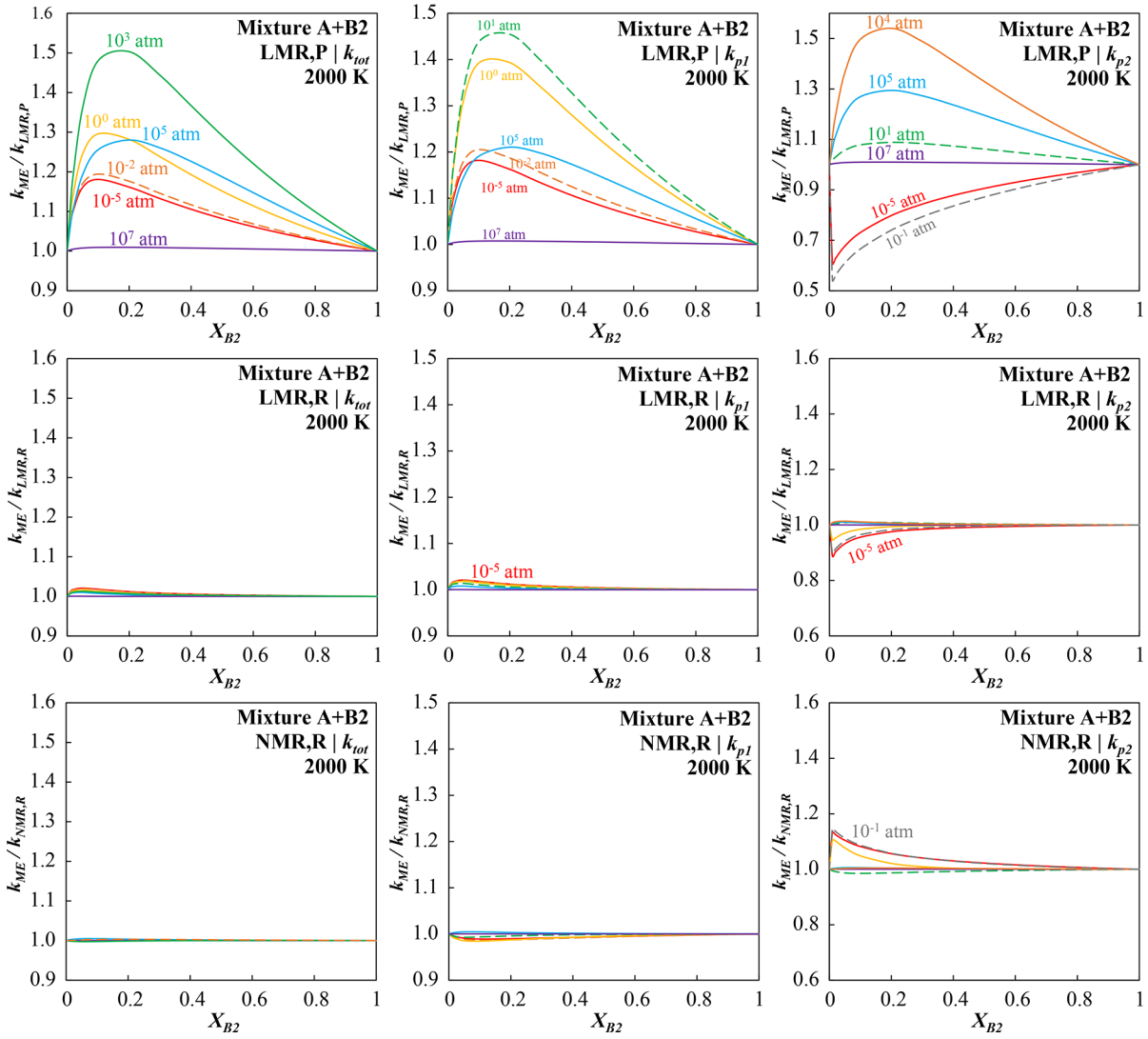

Figure 12. Comparisons of numerically calculated unimolecular rate constants and those estimated by various mixture rules (Table 2) at 2000 K for the CH_2O system (including tunneling) across various pressures for various two-component mixtures of A and B2 (Table 1). Different mixture rules are plotted in different rows: LMR,P (first row); LMR,R (second row); NMR,R (third row). Different channels are plotted in different columns: total reaction k_{tot} (first column); H_2 + CO, k_{p1} (second column); H + HCO, k_{p2} (third column).

in the mixture. Reinspection of the proof that rate constants for single-channel reactions are always underestimated by the linear mixture rule[30] reveals that the conclusion applies to the total rate constant for multichannel reactions. However, the linear mixture rule may underestimate or overestimate the channel-specific rate constants in the mixture depending on the channel (and the pressure).

(4) In contrast to single-channel reactions, the magnitude of the deviations from the linear mixture rule are not necessarily larger for larger differences in α_i among the colliders. For example, the magnitude of the deviations nonmonotonically depends on the differences in α_i between the colliders.

(5) The magnitude of the deviations from the linear mixture rule for some channels is larger, reaching ~30%, than those for the total rate constant, reaching ~10%. Furthermore, the sign of the deviations can be different for each channel, yielding errors in branching ratios among channels that reach ~50%.

(6) Analytical solutions of the master equation are in very good agreement with numerical solutions. This result indicates that the analytically derived activity coefficients provide an accurate representation of the nonlinear interactions among mixture components and, therefore, provide a reliable foundation for nonlinear mixture rules in the low-pressure limit.

With regard to general trends for multichannel reactions, the results also indicate the following across various pressures:

(1) Similar to results in single-channel reactions, the magnitude of deviations of the classic linear mixture rule (LMR,P) is largest in the intermediate falloff regime for all decomposition channels. The magnitude of LMR,P deviations for chemically activated reactions, which are influenced by the bath gas only at pressures above the low-pressure limit, is largest in the high-pressure limit. Deviations of LMR,P are observed for mixtures of colliders with different Z_i and/or different α_i.

(2) In contrast to single-channel reactions, the sign of deviations of the classic linear mixture rule (LMR,P) for some channel-specific rate constants can be different in different pressure regimes. For example, LMR,P overestimates k_{p2} at

DOI: 10.1021/acs.jpca.8b10581
J. Phys. Chem. A 2019, 123, 631−649

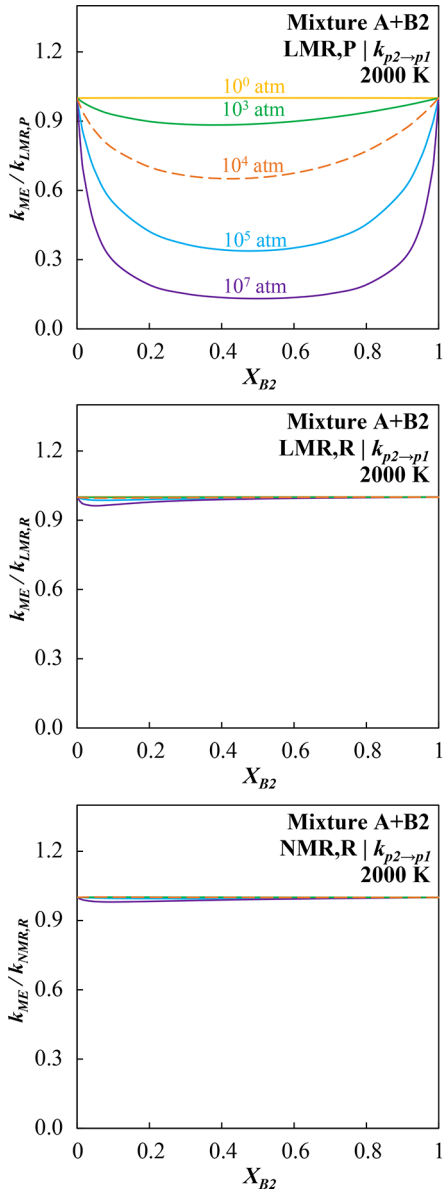

Figure 13. Comparisons of numerically calculated bimolecular rate constants ($k_{p2\rightarrow p1}$) from H + HCO (p2) to H_2 + CO (p1) and those estimated by various mixture rules (Table 2) at 2000 K for the CH_2O system (including tunneling) across various pressures for various two-component mixtures of A and B2 (Table 1). Different mixture rules are plotted in different rows: LMR,P (first row); LMR,R (second row); NMR,R (third row). Deviations for various mixture rules for other bimolecular channels (i.e., total bimolecular reaction, $k_{bi,tot}$, and H + HCO to CH_2O, $k_{p2\rightarrow w}$) are included in the Supporting Information.

lower intermediate pressures but underestimates k_{p2} at higher intermediate pressures.

(3) The magnitude of the deviations from the classic linear mixture rule (LMR,P) for some channels is larger (reaching a factor of ~50) than those for the total rate constant (reaching ~50%).

(4) Similar to results for single-channel reactions, new reduced-pressure-based mixture rules yield much better estimates of all decomposition and chemically activated rate constants in mixtures across all pressures, especially in the intermediate falloff regime. The linear reduced-pressure-based mixture rule (LMR,R) and nonlinear reduced-pressure-based mixture rule (NMR,R) are exact for all channels and all pressures for mixtures of components that differ only in Z_i but share the same α. For mixtures of components with different α_i, deviations of LMR,R are highest in the low-pressure limit, where they reach ~30% for some channels; deviations of NMR,R are essentially zero in the low-pressure limit and peak in the intermediate falloff regime, where they reach ~10% for some channels.

(5) In the new reduced-pressure-based mixture rules, when the rate constant for any channel is evaluated, including for chemically activated reactions, the reduced pressure is calculated according to the total decomposition rate constant rather than the channel-specific rate constants. (Use of the channel-specific rate constants instead was found to yield LMR,R deviations reaching a factor of ~4.) Similarly, use of an "effective low-pressure limit" total decomposition rate constant rather than the exact low-pressure limit total decomposition rate constant was also found to be an effective basis for evaluating mixture rate constants, as observed for the results where tunneling, which leads to an ill-defined low-pressure limit, was included in the calculations.

These new mixture rules are therefore recommended for use in fundamental and applied chemical kinetics investigations of reacting mixtures, including reacting flow codes and experimental interpretations of third-body efficiencies. For proper implementations of reduced-pressure-based mixture rules, it is recommended that future studies reporting channel-specific pressure-dependent rate constants for pure components, $k_{j,i}(T,P)$, also report, where possible, the total decomposition rate constants in the low- and high-pressure limits, $k_{0,i}(T)$ and $k_\infty(T)$. Furthermore, for implementation of the most accurate NMR,R, it is recommended that those studies also report α_i and Z_i for each collider and $F_E(T)$ for the reaction as per eq 11. In the meantime, mixture rules should be considered a significant structural uncertainty in chemical kinetics simulations and uncertainty quantification,[66−69] as discussed elsewhere.[69]

While the present calculations use the commonly employed exponential-down model to facilitate straightforward interpretations of the analytical solutions and to allow compatibility with the vast majority of calculated rate constants, which use the same model, improved quantification of mixture effects in future studies could be attained by using energy and angular momentum transfer functions determined via trajectory calculations and/or experimental measurements within a two-dimensional master equation. Naturally, as with rate constant calculations for even single-component bath gases for many pressure-dependent reactions, such mixture studies await such data to become available for a wider variety of bath gases and reactant complexes.

■ ASSOCIATED CONTENT

Supporting Information

The Supporting Information is available free of charge on the ACS Publications website at DOI: 10.1021/acs.jpca.8b10581.

Analytical solutions of activity coefficients for a two-component mixture; mixture rule performance (for calculations excluding and including tunneling) at 2000 K for channels not included in the main text, including graphical comparisons of calculated bimolecular rate constants; additional calculations of mixture

DOI: 10.1021/acs.jpca.8b10581
J. Phys. Chem. A 2019, 123, 631−649

rule performance at 3000 K, including a table of energy transfer parameters and graphical comparisons of calculated uni- and bimolecular rate constants; the chemically significant eigenvectors at 2000 K from calculations where tunneling was included (PDF)

Example input file for the CH_2O system used in the master equation calculations in the PAPR-MESS code[9] (using the potential energy surface from Klippenstein[54]) (TXT)

AUTHOR INFORMATION

Corresponding Author

*E-mail: mpburke@columbia.edu. Phone: +1 212-851-0782.

ORCID

Michael P. Burke: 0000-0002-1939-7824

Notes

The authors declare no competing financial interest.

ACKNOWLEDGMENTS

The authors gratefully acknowledge support of this research by the National Science Foundation through a grant from the Combustion and Fire Systems program (CBET-1733968) and the Donors of the American Chemical Society Petroleum Research Fund through a Doctoral New Investigator (DNI) award (PRF-56409-DNI-6). The authors also thank Stephen Klippenstein for sharing the theoretical data for the form-aldehyde system.[54]

REFERENCES

(1) Lindemann, F.; Arrhenius, S.; Langmuir, I.; Dhar, N.; Perrin, J.; Lewis, W. M. Discussion on "the radiation theory of chemical action". *Trans. Faraday Soc.* **1922**, *17*, 598−606.

(2) Hinshelwood, C. N. On the theory of unimolecular reactions. *Proc. R. Soc. London, Ser. A* **1926**, *113*, 230−233.

(3) Widom, B. Molecular transitions and chemical reaction rates. *Science* **1965**, *148*, 1555−1560.

(4) Quack, M.; Troe, J. In *Gas kinetics and energy transfer*; Ashmore, P. G., Donovan, R. J., Eds.; The Royal Society of Chemistry, 1977; Vol. 2, pp 175−238.

(5) Miller, J. A.; Klippenstein, S. J. Master equation methods in gas phase chemical kinetics. *J. Phys. Chem. A* **2006**, *110*, 10528−10544.

(6) Pilling, M. J.; Robertson, S. H. Master equation models for chemical reactions of importance in combustion. *Annu. Rev. Phys. Chem.* **2003**, *54*, 245−275.

(7) Barker, J. R.; Golden, D. M. Master equation analysis of pressure-dependent atmospheric reactions. *Chem. Rev.* **2003**, *103*, 4577−4592.

(8) Jasper, A. W.; Pelzer, K. M.; Miller, J. A.; Kamarchik, E.; Harding, L. B.; Klippenstein, S. J. Predictive a priori pressure-dependent kinetics. *Science* **2014**, *346*, 1212−1215.

(9) Georgievskii, Y.; Miller, J. A.; Burke, M. P.; Klippenstein, S. J. Reformulation and solution of the master equation for multiple-well chemical reactions. *J. Phys. Chem. A* **2013**, *117*, 12146−12154.

(10) Burke, M. P.; Klippenstein, S. J. Ephemeral collision complexes mediate chemically termolecular transformations that affect system chemistry. *Nat. Chem.* **2017**, *9*, 1078−1082.

(11) Maranzana, A.; Barker, J. R.; Tonachini, G. Master equation simulations of competing unimolecular and bimolecular reactions: Application to OH production in the reaction of acetyl radical with O_2. *Phys. Chem. Chem. Phys.* **2007**, *9*, 4129−4141.

(12) Olzmann, M.; Gebhardt, J.; Scherzer, K. An extended mechanism for chemical activation systems. *Int. J. Chem. Kinet.* **1991**, *23*, 825−835.

(13) Glowacki, D. R.; Lockhart, J.; Blitz, M. A.; Klippenstein, S. J.; Pilling, M. J.; Robertson, S. H.; Seakins, P. W. Interception of excited vibrational quantum states by O_2 in atmospheric association reactions. *Science* **2012**, *337*, 1066−1069.

(14) da Silva, G. Reaction of methacrolein with the hydroxyl radical in air: incorporation of secondary O_2 addition into the MACR+ OH master equation. *J. Phys. Chem. A* **2012**, *116*, 5317−5324.

(15) Burke, M. P.; Goldsmith, C. F.; Georgievskii, Y.; Klippenstein, S. J. Towards a quantitative understanding of the role of non-Boltzmann reactant distributions in low temperature oxidation. *Proc. Combust. Inst.* **2015**, *35*, 205−213.

(16) Barbet, M. C.; McCullough, K.; Burke, M. P. A framework for automatic discovery of chemically termolecular reactions. *Proc. Combust. Inst.* **2018**, DOI: 10.1016/j.proci.2018.05.002.

(17) Tardy, D. C.; Rabinovitch, B. S. Intermolecular vibrational energy transfer in thermal unimolecular systems. *Chem. Rev.* **1977**, *77*, 369−408.

(18) Oref, I.; Tardy, C. D. Energy transfer in highly excited large polyatomic molecules. *Chem. Rev.* **1990**, *90*, 1407−1445.

(19) Kee, R. J.; Rupley, F. M.; Miller, J. A. *Chemkin-II: A Fortran chemical kinetics package for the analysis of gas-phase chemical kinetics*; Sandia National Labs, 1989.

(20) Goodwin, D. G.; Moffat, H. K.; Speth, R. L. *Cantera: An object-oriented software toolkit for chemical kinetics, thermodynamics, and transport processes*, Version 2.3.0. http://www.cantera.org, 2017.

(21) Cuoci, A.; Frassoldati, A.; Faravelli, T.; Ranzi, E. A computational tool for the detailed kinetic modeling of laminar flames: Application to C_2H_4/CH_4 coflow flames. *Combust. Flame* **2013**, *160*, 870−886.

(22) Pitsch, H. *FlameMaster: A C++ computer program for 0D combustion and 1D laminar flame calculations*, Version 3.3.10; 1998.

(23) Chen, J. H.; Choudhary, A.; De Supinski, B.; DeVries, M.; Hawkes, E. R.; Klasky, S.; Liao, W.-K.; Ma, K.-L.; Mellor-Crummey, J.; Podhorszki, N. Terascale direct numerical simulations of turbulent combustion using S3D. *Comput. Sci. Discovery* **2009**, *2*, 015001.

(24) Poludnenko, A. Y.; Oran, E. S. The interaction of high-speed turbulence with flames: Global properties and internal flame structure. *Combust. Flame* **2010**, *157*, 995−1011.

(25) Bates, R. W.; Golden, D. M.; Hanson, R. K.; Bowman, C. T. Experimental study and modeling of the reaction $H+O_2+M \rightarrow HO_2+M$ (M = Ar, N_2, H_2O) at elevated pressures and temperatures between 1050 and 1250 K. *Phys. Chem. Chem. Phys.* **2001**, *3*, 2337−2342.

(26) Michael, J. V.; Su, M.-C.; Sutherland, J. W.; Carroll, J. J.; Wagner, A. F. Rate constants for $H+ O_2+ M \rightarrow HO_2+ M$ in seven bath gases. *J. Phys. Chem. A* **2002**, *106*, 5297−5313.

(27) Shao, J.; Choudhary, R.; Susa, A.; Davidson, D. F.; Hanson, R. K. Shock tube study of the rate constants for $H+ O_2+ M \rightarrow HO_2+ M$ (M= Ar, H_2O, CO_2, N_2) at elevated pressures. *Proc. Combust. Inst.* **2018**, DOI: 10.1016/j.proci.2018.05.077.

(28) Amedro, D.; Bunkan, A.; Crowley, J. *25th International Symposium on Gas Kinetics and Related Phenomena*; The Royal Society of Chemistry, 2018.

(29) Troe, J. Mixture rules in thermal unimolecular reactions. *Ber. Bunsenges. Phys. Chem.* **1980**, *84*, 829−834.

(30) Dove, J. E.; Halperin, S.; Raynor, S. Deviations from the linear mixture rule in nonequilibrium chemical kinetics. *J. Chem. Phys.* **1984**, *81*, 799−811.

(31) Schlag, E. W.; Valance, W. G. Theory of chemical reactions in mixtures with inert gases. *J. Chem. Phys.* **1968**, *49*, 605−609.

(32) Boyd, R. K. The linear mixture formula in non-equilibrium chemical kinetics. *Can. J. Chem.* **1977**, *55*, 802−811.

(33) Lim, C.; Truhlar, D. G. Study of mixture effects in the nonequilibrium kinetics of homonuclear diatomic dissociation and recombination. *J. Phys. Chem.* **1984**, *88*, 778−792.

(34) Tardy, D. C.; Rabinovitch, B. S. Collisional energy transfer. Thermal unimolecular systems in the low-pressure region. *J. Chem. Phys.* **1966**, *45*, 3720−3730.

(35) Tardy, D. C.; Rabinovitch, B. S. Collisional energy transfer in thermal unimolecular systems. Dilution effects and falloff region. *J. Chem. Phys.* **1968**, *48*, 1282−1301.

DOI: 10.1021/acs.jpca.8b10581
J. Phys. Chem. A 2019, 123, 631−649

(36) Schranz, H. W.; Nordholm, S.; Andersson, L. L. Pressure dependence of unimolecular reactions: Collision efficiencies in mixtures of weak and strong colliders. *Chem. Phys. Lett.* **1989**, *161*, 432−438.
(37) Carruthers, C.; Teitelbaum, H. The linear mixture rule in chemical kinetics. II. Thermal dissociation of diatomic molecules. *Chem. Phys.* **1988**, *127*, 351−362.
(38) Raynor, S.; Burke, K. Ab initio study of H_2 dissociation and vibrational relaxation in mixtures of He and Ar: Implications for the linear mixture rule. *J. Chem. Phys.* **1987**, *87*, 5788−5793.
(39) Schranz, H. W.; Nordholm, S.; Andersson, L. L. Theoretical analysis of collisional energy transfer in unimolecular reactions: Collision efficiencies in binary mixtures. *Chem. Phys.* **1990**, *143*, 25−38.
(40) Kiefer, J. H. Effect of VV transfer on the rate of diatomic dissociation. *J. Chem. Phys.* **1972**, *57*, 1938−1956.
(41) Burke, M. P.; Song, R. Evaluating mixture rules for multi-component pressure dependence: $H+O_2$ (+M)=HO_2 (+M). *Proc. Combust. Inst.* **2017**, *36*, 245−253.
(42) Lei, L.; Burke, M. P. Evaluating mixture rules and combustion implications for multi-component pressure dependence of allyl + HO_2 reactions. *Proc. Combust. Inst.* **2018**, DOI: 10.1016/j.proci.2018.05.023.
(43) Just, T.; Troe, J. Theory of two-channel thermal unimolecular reactions. 1. General formulation. *J. Phys. Chem.* **1980**, *84*, 3068−3072.
(44) Troe, J. Theory of thermal unimolecular reactions at low pressures. I. Solutions of the master equation. *J. Chem. Phys.* **1977**, *66*, 4745−4757.
(45) Rice, O. K. On the relation between an equilibrium constant and the nonequilibrium rate constants of direct and reverse reactions[1]. *J. Phys. Chem.* **1961**, *65*, 1972−1976.
(46) Rice, O. K. Further remarks on the "rate-quotient law". *J. Phys. Chem.* **1963**, *67*, 1733−1735.
(47) Miller, J. A.; Klippenstein, S. J. Some observations concerning detailed balance in association/dissociation reactions. *J. Phys. Chem. A* **2004**, *108*, 8296−8306.
(48) Oref, I.; Tardy, D. C. Energy transfer in highly excited large polyatomic molecules. *Chem. Rev.* **1990**, *90*, 1407−1445.
(49) King, K.; Barker, J. In *Unimolecular kinetics, Part 2: collisional energy transfer and the master equation*; Robertson, S., Ed.; Elsevier, 2019; Vol. *39*.
(50) Brown, N. J.; Miller, J. A. Collisional energy transfer in the low-pressure-limit unimolecular dissociation of HO_2. *J. Chem. Phys.* **1984**, *80*, 5568−5580.
(51) Lendvay, G.; Schatz, G. C. Comparison of master equation and trajectory simulation of the relaxation of an ensemble of highly vibrationally excited molecules. *J. Phys. Chem.* **1994**, *98*, 6530−6536.
(52) Barker, J. R.; Weston, R. E. Collisional energy transfer probability densities P(E, J; E′, J′) for monatomics colliding with large molecules. *J. Phys. Chem. A* **2010**, *114*, 10619−10633.
(53) Jasper, A. W.; Miller, J. A. Collisional energy transfer in unimolecular reactions: Direct classical trajectories for CH_4 = CH_3 + H in Helium. *J. Phys. Chem. A* **2009**, *113*, 5612−5619.
(54) Klippenstein, S. J. Personal communication.
(55) Troe, J. Refined analysis of the thermal dissociation of formaldehyde. *J. Phys. Chem. A* **2007**, *111*, 3862−3867.
(56) Troe, J. Analysis of quantum yields for the photolysis of formaldehyde at λ > 310 nm. *J. Phys. Chem. A* **2007**, *111*, 3868−3874.
(57) Klippenstein, S. J.; Georgievskii, Y.; Harding, L. B. Statistical theory for the kinetics and dynamics of roaming reactions. *J. Phys. Chem. A* **2011**, *115*, 14370−14381.
(58) Townsend, D.; Lahankar, S. A.; Lee, S. K.; Chambreau, S. D.; Suits, A. G.; Zhang, X.; Rheinecker, J.; Harding, L. B.; Bowman, J. M. The roaming atom: straying from the reaction path in formaldehyde decomposition. *Science* **2004**, *306*, 1158−1161.
(59) Fernandes, R. X.; Luther, K.; Troe, J.; Ushakov, V. G. Experimental and modelling study of the recombination reaction H+ O_2 (+ M) →HO_2 (+ M) between 300 and 900 K, 1.5 and 950 bar, and in the bath gases M= He, Ar, and N_2. *Phys. Chem. Chem. Phys.* **2008**, *10*, 4313−4321.
(60) Forst, W. Tunneling in thermal unimolecular reactions. Formaldehyde. *J. Phys. Chem.* **1983**, *87*, 4489−4494.
(61) Troe, J. Predictive possibilities of unimolecular rate theory. *J. Phys. Chem.* **1979**, *83*, 114−126.
(62) Troe, J.; Ushakov, V. G. Revisiting falloff curves of thermal unimolecular reactions. *J. Chem. Phys.* **2011**, *135*, 054304.
(63) Troe, J. Fall-off curves of unimolecular reactions. *Ber. Bunsen-Ges. Phys. Chem.* **1974**, *78*, 478−488.
(64) Barker, J. R.; Ortiz, N. F. Multiple-well, multiple-path unimolecular reaction systems. II. 2-methylhexyl free radicals. *Int. J. Chem. Kinet.* **2001**, *33*, 246−261.
(65) Just, T. Multichannel reactions in combustion. *Symp. (Int.) Combust., [Proc.]* **1994**, *25*, 687−704.
(66) Olm, C.; Varga, T.; Valkó, Éva; Curran, H. J.; Turányi, T. Uncertainty quantification of a newly optimized methanol and formaldehyde combustion mechanism. *Combust. Flame* **2017**, *186*, 45−64.
(67) Tao, Y.; Smith, G. P.; Wang, H. Critical kinetic uncertainties in modeling hydrogen/carbon monoxide, methane, methanol, formaldehyde, and ethylene combustion. *Combust. Flame* **2018**, *195*, 18−29.
(68) Slavinskaya, N. A.; Abbasi, M.; Starcke, J. H.; Whitside, R.; Mirzayeva, A.; Riedel, U.; Li, W.; Oreluk, J.; Hegde, A.; Packard, A.; Frenklach, M.; Gerasimov, G.; Shatalov, O. Development of an uncertainty quantification predictive chemical reaction model for syngas combustion. *Energy Fuels* **2017**, *31*, 2274−2297.
(69) Burke, M. P. Harnessing the combined power of theoretical and experimental data through multiscale informatics. *Int. J. Chem. Kinet.* **2016**, *48*, 212−235.

DOI: 10.1021/acs.jpca.8b10581
J. Phys. Chem. A 2019, 123, 631−649